Analysis of heat transfer and fluid flow in an evaporating sessile droplet for evaporative cooling applications.

by

Md. Almostasim Mahmud

A Thesis Submitted in Partial Fulfillment

of the Requirements for the Degree of

Master of Applied Science

in

Mechanical Engineering

Department of Automotive, Mechanical and Manufacturing Engineering
Faculty of Engineering and Applied Science
University of Ontario Institute of Technology

August, 2015

Abstract

Cooling is of critical importance for a number of fields, particularly in microelectronic devices and other miniaturized technology. The evaporation of the sessile liquid droplet facilitates the phase change of that liquid and provides cooling to the system, because a large amount of latent heat is required to change the phase. Evaporation takes place at the liquid-vapour interface, so to enhance the phase change process, it is essential to understand the interfacial energy transport mechanisms involved in transporting energy to the liquid-vapour interface from the solid substrate and the vapour surrounding. A series of experiments were conducted under different experimental conditions to understand interfacial energy transport in an evaporating sessile droplet. The experimental results demonstrate the effect of the ambient and substrate temperature on the evaporation process and the relative contributions of the conduction energy transport and other modes of energy transport in the total energy required for the phase change process.

Keywords: evaporation, sessile droplet, cooling, phase change

Acknowledgements

I would like to express my sincere gratitude to my supervisor Dr. Brendan MacDonald for his continuous support, encouragement and guidance throughout the research work. He gave me the opportunity to work in his research team when I was looking for that. He taught me essential research skills from scratch and guided me to develop my natural ability. He has been very welcoming and positive, and that is what made the entire research team confident and motivated.

I would like to thank all the members of the *Macdonald Lab*: Noosheen Walji, Mosfera Chowdury, Soma Chakraborty, Anders Nielsen and Han Wu for their cooperation and support. A special thanks to Noosheen Walji, who helped me to understand different aspects of a new society. I would like to thank Han Wu for helping me to buy the digital camera for the experimental setup.

I would like to thank my mother, Mostari Mahmud, who has been helping me and guiding me throughout my life, and who is always available to pick up the phone when I call her. I would like to thank my sister, Zakia Sultana and her little son Ayman Muhammad, who make me happy when I talk with them.

Contents

List of Tables

List of Figures

Nomenclature

$(\Delta h_{vap})_{T=T_i}$	Enthalpy of vaporization at the interfacial temperature
i_r	Unit vector perpendicular to the interface along the radial direction
$j_{ev}(\emptyset)$	Local evaporation flux associated with the conduction energy transport
J_{ev}	Total evaporation rate associated with the conduction energy transport
J_{actual}	Actual evaporation rate obtained from syringe pump
k_L	Thermal conductivity of liquid
k_V	Thermal conductivity of vapour
r	Radial distance
r_i	Radius of the droplet (Radial distance of the interface)
T^V	Vapour phase temperature
T^L	Liquid phase temperature
T_i^V	Vapour phase temperature at the interface
T_i^L	Liquid phase temperature at the interface
$\emptyset$	Polar angle

Chapter 1

1 INTRODUCTION

1.1 Motivation

Thermal management of microelectronic devices is considered as a crucial design challenge. Compact design and high data processing speed are the main demands from the user end and they require high heat removal rate from a small surface area. An effective thermal management system, capable of regulating the temperature within the operating range, is a prerequisite of compact design. A microelectronic device, such as the data processing unit of a computer, generates a large amount of heat and it increases with the processing speed. The conventional cooling systems, such as the air cooling system with metal fins, have been struggling to keep pace with the increasing cooling demand. Therefore an effective thermal management solution can facilitate the design of future microelectronic devices.

An evaporative cooling system, incorporating evaporation of sessile droplets on a hot substrate, can be implemented in the thermal management system of the

microelectronic devices. In the evaporation process, the phase change from the liquid to the vapour extracts a large amount of heat from the droplet and provides cooling. Nature also provides the examples of a similar cooling strategy, such as the human body cooling through perspiration, where sessile droplets (sweat) evaporate on the skin and provide cooling in situations with high heat removal requirements. In addition, some animals who do not have sweat glands like human being also use different strategies of evaporative cooling. During the hot summer, dogs regulate their body temperature through the evaporative cooling of their tongue, elephants spray water on their body by their trunk to facilitate evaporative cooling. All these examples of the cooling strategy used by the nature, indicate the potential of evaporative cooling systems in practical applications.

1.2 Comparative advantages of evaporative cooling

Conventional cooling systems are based on the vapour-compression refrigeration cycle. In the refrigeration cycle, the refrigerant changes its phase from liquid to vapour in the evaporator by extracting heat from the heat source and provides cooling; similarly, in the condenser it changes its phase from vapour to liquid by rejecting heat to the heat sink. This is how it transfers the heat energy from low temperature heat source to the high temperature heat sink. To do so, it requires high compressor power to maintain a pressure differential between the evaporator and

condenser. In contrast, evaporative cooling is a natural phase change phenomenon that does not require any compressor power, and it can transfer heat energy from heat source in the form of mass transfer. All the natural evaporative cooling systems mentioned in the previous paragraph, show how phase change of liquid provides cooling. Therefore, to transfer heat energy from the heat source to the heat sink, an evaporative cooling system can be the effective mechanism in some applications. In addition, the refrigerants used in the refrigeration cycle have high global warming potential, so it is not a green technology, and some parts of the world do not have enough electrical power supply to power appliances with the refrigeration cycle. Under these circumstances, the refrigeration cycle cannot be the only solution for the cooling applications. In contrast, an evaporative cooling system can be designed by the evaporation of normal water; but to enhance the mass transfer, it may need an electric fan. However, the power consumption of an electric fan is very low compared to the power consumption of the compressor. Therefore, the evaporative cooling system has the potential to be implemented in cooling applications where it is best suited.

1.3 Evaporative air cooling

It is explained in the section 1.1 that evaporative cooling system has the potential to be implemented in the applications related to hot surface cooling. However, air

can also be cooled by the evaporative cooling system. With the advancement of technology a large number of electric appliances and machineries have been used in indoor spaces. In these cases, the indoor space is used as the heat sink for those appliances and machineries, and that eventually increase the space air temperature according to the process of the sensible heating. In addition, in hot countries, indoor spaces with the concrete wall become heated up by sunlight and increases the space temperature. To deal with this situation, the countries with sufficient electric power supply have been maintaining controlled temperature using the refrigeration cycle. However, the countries with inadequate power supply, cannon facilitate refrigeration cooling system and the people of those countries have been experiencing uncomfortable, unproductive and unhealthy hot and dry indoor environment. For example, in Bangladesh workers have been working in some factories where indoor space temperature is as high as 45℃. This situation is common in almost all the factories where they work with high temperature machineries, such as plastic and ceramic industries of Bangladesh. A water based evaporative cooling system, can maintain a colder and moderately humid indoor air under these situations. Another advantage of this type of cooling system is that, it allows natural flow of air from outside as it does not work under air tight indoor space, whereas cooling with refrigeration cycle is designed for air tight indoor spaces with the minimum

circulation of outside air. Therefore an evaporative cooling system can be used in the indoor air cooling applications, particularly in those parts of the world where power supply is inadequate and the environment is hot and dry.

1.4 Principle of evaporation

Evaporation is a surface phenomenon, it takes place at the interface of liquid and vapor phases, shown in the Figure 1.1. At the molecular level, there is no such well-defined boundary in between the liquid and vapor phase, rather there is layer that is a few molecules thick called the Knudsen layer [1, 2]. The thin liquid layer along the periphery of base circle, which is in contact with both solid and gaseous phase, is termed the three phase contact line. During this process, liquid molecules gain a certain level of the kinetic energy and leave the interface [3].

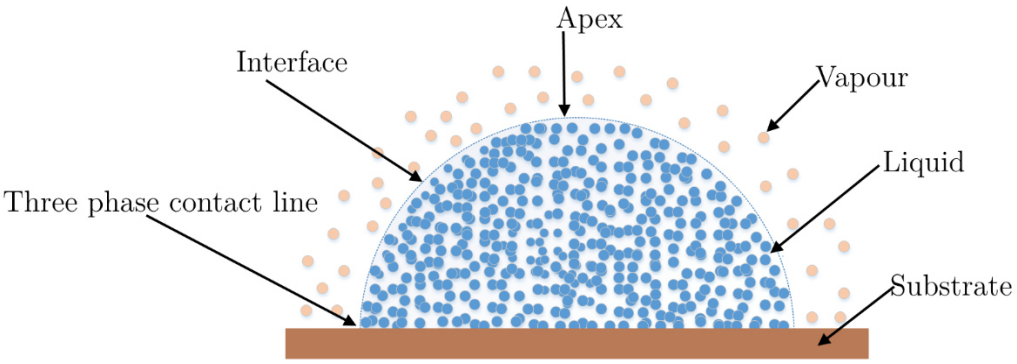

Figure 1.1 A sessile droplet evaporating on the hot substrate

At a high enough energy level the liquid molecules transform their liquid phase into the vapour phase and extract the latent heat of evaporation from the interface, this

is illustrated in Figure 1.1.The evaporation rate depends on the available energy at the interface to enable the phase change. The required latent heat of evaporation can be provided by either the gaseous medium or from the liquid medium or both [4]. Therefore the evaporation rate of the sessile droplet depends on the energy transport mechanisms that transport energy to the interface, from the substrate and/or the surrounding medium.

1.5 Evaporation flux distribution

During the evaporation of a sessile droplet, the evaporation rate varies with the different regions of the droplet surface. To take this physical phenomenon into the consideration, in a small surface area of the droplet, a term representing the local evaporation rate per unit area is considered for the calculation of the total evaporation rate from the droplet surface. This term is known as the local evaporation flux. Since the droplet is axisymmetric around the vertical axis 'z', shown in Figure 1.2, the variations in the local evaporation flux from the apex of the droplet to the three phase contact line represent the complete evaporation profile of the droplet, shown in Figure 1.1. This distribution of the local evaporation flux from $\emptyset = 0°$ to $\emptyset = 90°$ is commonly known as the evaporation flux distribution.

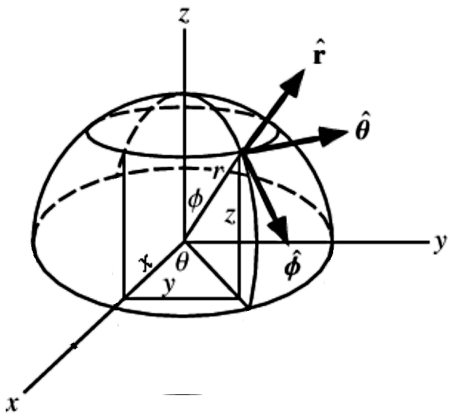

Figure 1.2 the spherical coordinate system used in the calculation the spherical sessile droplet.

1.6 Interfacial energy transport

A high evaporation rate indicates high energy transport to the interface. The higher rate of the energy transport from the substrate to the interface, corresponds to higher cooling rate of the substrate, which is essential for the hot substrate cooling, such as the microelectronic cooling. Similarly a high rate of energy transport from the surrounding gaseous medium to the interface can cause the cooling of that medium, such as the evaporative air cooling. The energy required for the evaporation can be transported to the interface through the bulk liquid phase and/or through the vapour phase surrounding the sessile droplet. A proper understanding of the interfacial energy transport mechanisms can lead to higher evaporation rates, and it will facilitate the design of effective evaporative cooling systems.

1.6.1 Energy transport through the liquid phase

In a sessile droplet, the energy transport through the liquid phase depends on the thermal conduction and/or internal convective flows, such as Marangoni flow and buoyancy driven flow. The temperature profile of the bulk liquid can be used to calculate the rate of the conduction energy transport to the interface and to determine the directions of the probable internal convections inside the droplet.

The thermal conduction through the bulk liquid of a spherical sessile droplet, depends on the temperature profile of the liquid phase along its radial direction, perpendicular to the interface. The temperature gradient at the interface along this direction $\left(\frac{dT^L}{dr}\right)_{r=r_i}$, indicates the direction and magnitude of the energy transport to the interface. A negative temperature gradient indicates the energy contribution of the liquid phase to the interface and a positive temperature gradient indicates heat conduction away from the interface. In addition, a gradient in the surface temperature of the droplet $\left(\frac{dT^L}{d\emptyset}\right)_{r=r_i}$ from the droplet apex to the three phase contact line, indicates the directions of surface tension driven flows. Therefore temperature profile of the liquid phase along the radial direction and along the droplet surface, provides substantial evidence about the mechanisms of the energy transport to the interface through the liquid phase.

There are some other physical parameters that can affect the conduction energy transport through the liquid phase, such as the liquid thermal conductivity, droplet shape, size of the droplet, and substrate thermal conductivity.

1.6.2 Energy transport through the vapour phase

The energy transport through the vapour phase can be governed by the thermal conduction as well as the convection. However, in case of droplet evaporation inside of an enclosure with no forced air flow, convection in the vapour phase can be neglected. Same as the liquid phase, the direction and magnitude of conduction energy transport through the vapour phase surrounding the droplet, to or from the interface, depends on its temperature gradient at the interface along the radial direction$\left(\frac{dT^V}{dr}\right)_{r=r_i}$. Unlike the liquid phase, a positive temperature gradient indicates the energy contribution of the vapour phase to the interface and a negative temperature gradient indicates heat conduction through the vapour phase away from the interface.

1.6.3 Conduction dominant energy transport

To implement the evaporative cooling system in practical applications, it is crucial to understand the dominant energy transport mechanism under certain situation. The cooling system needs to be designed based on the dominant mode of energy

transport in that particular situation. If the conduction energy transport mode is dominant in both the liquid and vapour phases, and the other modes of the energy transport are negligible, then there will be an energy balance between the overall energy transported to the interface by the conduction energy transport through liquid phase and vapour phase, and the total energy required for the evaporation. The energy balance for the local evaporation flux can be written as:

$$\left\{ \; k_V \left(\frac{dT^V}{dr}\right)_{r=r_i} - \; k_L \left(\frac{dT^L}{dr}\right)_{r=r_i} \right\} \cdot \; i_r = j_{ev}(\emptyset) \cdot (\Delta h_{vap})_{T=T_i} \qquad (1)$$

Where, k_V and k_L are the thermal conductivity of vapour and liquid respectively; $j_{ev}(\emptyset)$ is the local evaporation flux associated with the conduction energy transport; $(\Delta h_{vap})_{T=T_i}$ is the enthalpy of vaporization at the interfacial temperature; i_r is the unit vector perpendicular to the interface; and $\left(\frac{dT^V}{dr}\right)_{r=r_i}$ and $\left(\frac{dT^L}{dr}\right)_{r=r_i}$ are the temperature gradient of the vapour and liquid phases at the interface measured from their temperature profile. This equation can be used to calculate the local evaporation flux $'j_{ev}(\emptyset)'$ associated with the conduction.

The total evaporation rate associated with the conduction can be calculated by integrating the local evaporation flux throughout the droplet surface, sign conventions are shown in Figure 1.2.

$$J_{ev} = \int_0^{2\pi} \int_0^{\pi/2} j_{ev}(\emptyset) \cdot {r_i}^2 \cdot sin\emptyset d\emptyset d\theta \qquad (2)$$

Here, J_{ev} is the total evaporation rate from the droplet associated with the conduction energy transport; r_i is the radius of the spherical droplet; and $\emptyset$ and θ are the polar angle and the azimuthal angle respectively. If J_{ev} is equal to the actual evaporation rate, J_{actual} , then it can be concluded that the total energy required at the interface to maintain the actual rate of evaporation is transported by the conduction through the liquid phase and the vapour phases. This situation is considered as the energy balance situation with the conduction energy transport. However, if the evaporation situation is not dominated by the conduction energy transport, there will be an imbalance and this imbalance indicates the contribution of other energy transport mechanisms in the evaporation. In this situation, the convective internal flows in the droplet, the radiation energy transport from the surroundings or energy transport from other phenomena can act as the interfacial energy transport mechanism.

1.7 Internal convection in a sessile droplet

In the previous section it was discussed that the liquid phase can transport energy to the interface through the conduction as well as the internal convective flows. Primarily there are two types of convective flow that occur inside a droplet, one is Marangoni flow and another one is Buoyancy driven flow.

1.7.1 Marangoni flow

Marangoni flow occurs due to the surface tension gradient induced at the interface, the region with higher surface tension pulls the liquid layer from the region of lower surface tension, which is termed the Marangoni effect [5]. The surface tension gradient can be created by the temperature gradient or the concentration gradient [6]. The Marangoni flow induced by temperature gradient is termed as thermocapillary flow [6]. During the evaporation of a sessile droplet, the local evaporation fluxes are not uniform throughout the interface, this kind of uneven local evaporation flux creates a temperature gradient over the droplet surface and thus the thermocapillary convection occurs in the droplet [7]. However, if thermocapillary stress is less than the viscous shear stress then the effect of the surface tension force can be neglected [8]. If a pure liquid is used in the sessile droplet, then the concentration gradient is negligible.

1.7.2 Buoyancy driven flow

In an evaporating sessile droplet, if the liquid layer close to the droplet apex becomes heavier than the liquid layer of the bottom of the droplet, then the heavier liquid layer slides over the lighter layer of the liquid and creates a convective flow inside the droplet, because a heavier liquid layer on a light liquid layer creates instability.

This type of convective flow is termed buoyancy driven flow. In an experimental condition where the substrate temperature is high and the ambient is low, the droplet apex is colder than the bottom side of the droplet due to the evaporation, and a colder liquid layer corresponds larger density which creates heavier liquid layer. In this case, a buoyancy driven flow occurs inside the droplet. However, the effect of buoyancy driven flow can be reduced by making the droplet small, because buoyancy is a body force which depends on the volume of the droplet.

1.8 Droplet Geometry

Depending on the situation, a liquid droplet can have a different shape. A liquid droplet can have a geometry of a sphere if the liquid is sprayed in free space, this type of droplet is commonly termed a 'free droplet'. In some evaporative air cooling applications, a water spraying nozzle is used to form tiny droplets in the air, these kind of applications require proper understanding of the evaporation dynamics of a free spherical droplet. In contrast, when a liquid droplet is placed on a solid substrate, this type of droplet is termed a 'sessile droplet'. In the applications where sessile droplets are used to cool down a hot surface, such as the microelectronic cooling, require proper understanding of the evaporation dynamics of the sessile droplet.

A sessile droplet tends to form a shape of a sphere on the substrate, depending on the properties of the surface, the contact angle of the droplet can be more or less than 90°. If the contact angle is equal to 90° then this type of sessile droplet is commonly called a 'spherical droplet' and if the contact angle is less than 90° then it is called a 'spherical cap droplet' as shown in the Figure 1.3.

1.8.1 Spherical droplet

The conduction energy transport in a spherical droplet follows established equations of thermal conduction in spherical coordinates. Therefore, the interfacial conduction energy transport both from the liquid and the vapour phase can be calculated by applying these equations. To do so, it requires the temperature profiles of the liquid phase and vapour phases in both sides of the interface.

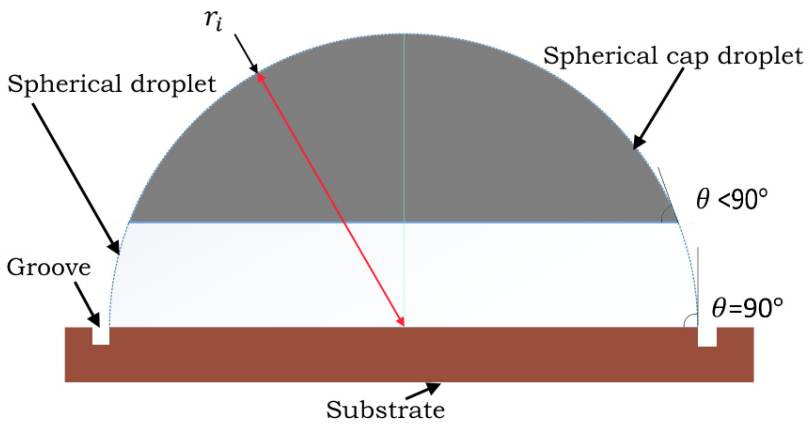

Figure 1.3 Spherical and spherical cap shape of the sessile droplet

A liquid droplet forms a certain contact angle on a specific solid surface. However, this contact angle can be manipulated by surface treatments. Another effective method of generating a spherical droplet is to make a circular groove on the solid surface around the droplet, the edge of the groove forces the droplet three phase contact line.

1.8.2 Spherical cap droplet

The conduction energy transport in a spherical cap does not follow the conduction equations of spherical coordinate, because the boundary conditions for a spherical droplet do not match with the boundary conditions of a spherical cap droplet. Therefore the sessile droplet needs to be spherical to measure the conduction energy transport to the vapour-liquid interface applying the conduction equations of spherical coordinate.

Chapter 2

2 RECENT WORK IN THE FIELD

It was noted in the introduction that evaporation takes place at the liquid-vapour interface where the liquid molecules transform into the vapour molecules by absorbing the required energy from the interface. To implement evaporating droplet technology in cooling applications, the evaporation rate needs to be maximized for the operating conditions. To meet this requirement, researchers have been working to understand the evaporation dynamics and the modes of interfacial energy transport that affect the rate of evaporation. At the same time, research work has been done on different probable applications of this technology. The large number of published work and the involvement of research groups from all over the world show the potential of this technology.

2.1 Work on 'Evaporation rate'

In the evaporative cooling applications, evaporation rate corresponds to the cooling rate. Therefore research work have been done to understand the factors associated with the evaporation rate .The evaporation rate of a sessile droplet depends on the local evaporation flux, which is discussed in the introduction, so the overall evaporation rate of the droplet can be maximized by enhancing the local evaporation flux throughout the droplet surface. Research work has been done to understand and enhance evaporation rate. The local evaporation flux has been considered as tool to optimize the evaporation rate.

In 1999, an experimental work [9] was done by C.A. Ward et al. to observe the evaporation of a liquid layer under a pressure range of 290 Pa to 1030 Pa and a temperature range of 1 ℃ to 4℃ , where water was used as the liquid. They observed that there is a temperature discontinuity at the interface between the vapour phase and the liquid phase, where at the interface the vapour phase temperature is higher than the liquid phase along the droplet surface. They measured the evaporation rate experimentally and experimental results agreed with their theoretical prediction of evaporation rate based on the statistical rate theory (SRT).

In the same year, the evaporation dynamics of a spherical interface was observed experimentally by G. Fung and C. A. Ward [10]. They formed a spherical liquid layer at the mouth of a conical funnel to observe the evaporation from a spherical interface. The temperature of the liquid and the vapour phases were measured by a miniature thermocouple of 25.4 μm diameter. Two different hydrocarbons were used as the liquid and the experiments were conducted under a pressure range of 480 Pa to 3000 Pa, and a chamber temperature of around 26℃. From this experiment they found a temperature discontinuity of 4℃ and the vapour phase temperature is higher than the liquid phase along the interface.

In 2001, C. A. Ward and D. Stanga experimentally investigated [11] both the evaporation and condensation processes using the same conical funnel with a mouth opening of 7mm and water was used as the liquid. They conducted the experiments with a pressure range of 600 pa to 2000 Pa, a temperature range of -4℃ to 26℃ depending on the evaporation and condensation situation. Buoyancy driven flow was eliminated in their experiment. In this experiment, they observed the temperature discontinuity where the vapour phase temperature is higher than the liquid phase temperature. In addition, they observed a liquid layer of uniform temperature just below the interface. They recommended that this uniform temperature layer should be taken into the account to measure the temperature discontinuity.

In 2002, H. Hu and R.G. Larson [12], conducted an experimental analysis followed by the numerical prediction, to measure the evaporation rate of a spherical cap shape pinned water droplet on a glass substrate, under the atmospheric pressure and the room temperature. They used a florescence microscope to measure the time dependant change in droplet shape and proposed an empirical expression to calculate the evaporation rate as a function of contact angle. They didn't consider the thermocapillary flow for their analysis.

In 2007, S. David and K. Sefiane [13], experimentally investigated the effect of substrate thermal conductivity on the evaporation rate of a sessile water droplet under reduced a pressure environment. The temperature profile of the liquid phase of a spherical cap shape droplet was measured by a miniature thermocouple. They observed that an insulating substrate offers a cooling effect in the droplet and the rate of evaporation increases with the thermal conductivity of the substrate.

In 2008, another theoretical analysis on the effect of substrate and liquid thermal conductivities on a pinned spherical cap shape droplet was done by G.J Dunn and K. Sefiane[14]. They used multiple materials with wide range of thermal conductivities and the entire experiment was conducted under room temperature and

atmospheric pressure. They predicted that, the thermal conductivity of both the liquid and the substrate affect the evaporation rate. They found high local evaporation flux near the three phase contact line, whereas the thermocapillary flow was not taken into consideration.

In 2009, G.J. Dunn et el. with K. Sefiane [15], demonstrated the strong effect of substrate thermal conductivity on the evaporation of a spherical cap shape pinned droplet under atmospheric pressure. The temperature of the substrate was maintained at 22℃, and different types of liquids and substrates were used for the investigation. They observed high evaporation flux near the three phase contact line and proposed a theoretical model to predict those experimental conditions.

In 2009, K. Sefiane et al. [16], experimentally investigated the effect of atmosphere on the evaporation of a spherical cap shape and pinned sessile water droplet under reduced pressure of 40 mbar to 1000 mbar. They used different ambient gases and substrate materials for the investigation and the temperature of the liquid phase was measure by a miniature thermocouple. They developed a theoretical model to predict the evaporation rate and found good agreement with the experimental results. However, they concluded that at higher evaporation rate their model does not provide an accurate prediction.

In 2010, Fabien Girard and K. Sefiane [17], conducted an experimental analysis on a millimetre sized sessile water droplet on a heated substrate (30 to 60 ℃) under atmospheric pressure and room temperature of 20℃, to measure the local evaporation flux and interfacial temperature distribution. They used infrared thermography to measure interfacial temperature distribution and the data were validated by the optical measurement. They found the temperature gradient between the apex and the three phase contact line, and the evaporation flux near the three phase contact line was the maximum.

2.2 Work on 'Internal flow in evaporating sessile droplet'

Research work has been done on the internal flows in evaporating sessile droplet, primarily for two reasons: (a) to understand its effect on the evaporation rate; (b) to understand its effect on pattern formation by dried out droplets. Some relevant work on the internal flows in a sessile droplet will be listed in this section.

In 2005, H. Hu and R.G. Larson [18] theoretically predicted the flow field inside a spherical cap shape pinned evaporating droplet. They proposed theoretical model both for the evaporation with and without the thermocapillary flow to predict the flow pattern during slow evaporation.

In 2007, X. Xu and J. Luo [19] experimentally observed the Marangoni flow in a evaporating water droplet. For the experiment they used fluorescent particle, a spherical cap shape droplet, deionized water as liquid, and the experiment was conducted with a substrate temperature of 28℃, the ambient relative humidity of 60% and at atmospheric pressure. They observed that the surface tension force changes its direction along the interface and creates a '*stagnation point'* near the three phase contact line.

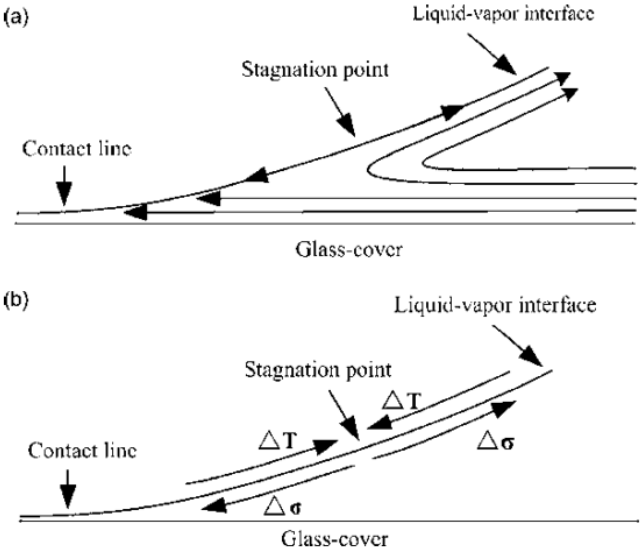

Figure 2.1 (a) Flow pattern sketch in the region near the contact line of the liquid droplet. (b) Temperature gradient and surface tension greadient along the surface [19].

In 2008, Fabien Girard et al. [20] numerically investigated the effect of heated substrate on the evaporation of a spherical cap shape water droplet. They predicted

the probable direction and pattern of the thermocapillary convection under different temperature and the size of the heating element.

In 2009, Victor Starov and K. Safiane [21], conducted a numerical analysis on the evaporation of a sessile droplet under ambient temperature and atmospheric pressure. They observed a linear dependency of the evaporation rate on the droplet base radius. They also predicted that, the interfacial temperature gradient leads to thermocapillary flow and established a relation between the local evaporation flux and the interfacial temperature.

In 2010, John Christy et al. with K. Sefiane [22], experimentally investigated the flow pattern inside a pinned liquid droplet evaporating on a non-heated substrate under atmospheric pressure and room temperature. They used water and methanol as liquid and the micro-PIV (Particle Image Velocimetry) system was used to visualize the flow. They observed maximum liquid phase velocity near the three phase contact line.

In 2010, K. Sefiane [23], conducted a different experimental analysis on the pattern formation by the nanoparticles of an evaporating sessile droplet when it dries out. He observed and analyzed patterns under different substrate temperature (20 to

80 ℃) and different concentrations of the nanoparticles in the liquid. He explained the potential of evaporative pattern formation technology in biomedical applications.

In 2010, X. Xu et al. [24] theoretically predicted the Marangoni flow induced by non-uniform surface temperature in an evaporating sessile droplet. They found that the direction of the Marangoni flow not only depends on the relative thermal conductivity of the liquid and the substrate, also depends on the ratio of the substrate thickness and contact line radius.

In 2011, Brendan D. MacDonald and C.A. Ward [25], investigated the onset criterion of thermocapillary flow in the spherical interface formed at the mouth of the funnel. They introduced a stability parameter to predict the stable evaporation under the conductive and the insulating surface of the funnel. In 2012, in another study, Brendan D. MacDonald and C.A. Ward [26] theoretically analyzed the onset criterion of the thermocapillary flow in an evaporating sessile droplet both for the conductive and insulating substrate. In both studies, they introduced two stability parameters to predict the stable evaporation under those two experimental conditions. The stability parameters were free of fitting variables and that made it useful to predict other evaporation conditions. Each theoretical prediction was verified with experimental investigation and the experimental data were found to be consistent with the prediction. From study on funnel they concluded that smaller

interfacial discontinuities, higher evaporation rate, and smaller radii corresponds to less stable system. Whereas in an evaporating sessile droplet they concluded that smaller interfacial temperature discontinuities, higher evaporation rate and smaller droplets correspond to less stable systems

In 2014, X. Xu et al.[27] experimentally observed the linear growth of the colloidal rings at the edge of pinned **drying droplets** under room temperature and atmospheric pressure. In this study, they observed two different type of flow, Marangoni convection and capillary outward flow, and they mentioned that particles can be deposited by the capillary outward flow as well, below the stagnation point.

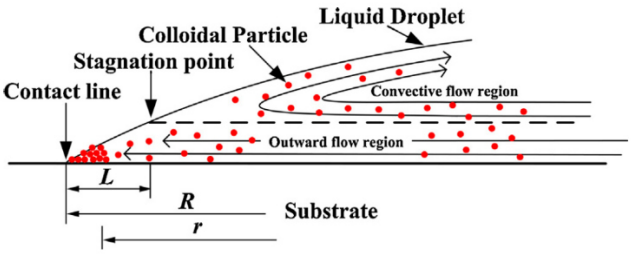

Figure 2.2 Sketch of the flow field inside a pinned spherical droplet [27].

In 2015, X. Xu et al. [28] theoretically analyzed the effect of evaporative cooling on the bulk liquid in a drying droplet. They specified the situations when it is important to consider evaporative cooling effect on the drying droplet.

2.3 Work on the 'Interfacial energy transport'

Enhancement of the local evaporation flux requires a proper understanding of the modes of energy transport to the interface, the effect of substrate properties, the effect of liquid properties, the effect of the temperature discontinuity at the interface, and the effect of ambient thermodynamic conditions. Researchers have been working on the different evaporation and condensation conditions where liquid and vapour phases are involved. They have been looking at the modes of interfacial energy transport, the effect physical properties of the liquid and vapour phases at the interface, the effect of the physical properties of the substrate and other relevant factors that can affect the evaporation process [29].

In 2004, C.A. ward and Fei Duan [30] experimentally observed the effect of thermocapillary flow on the conduction energy transport. They investigated evaporation of a spherical interface at the mouth of a funnel and buoyancy force was eliminated in the setup. A 12.7 μm probe was used to measure the interfacial flow velocity, funnel throat temperature was maintained at 3.56 ℃ and experimental pressure was maintained within a pressure range of 200 Pa to 800 Pa. They concluded that thermocapillary flow plays an important role in the energy transport and any strong thermocapillary flow parallel to the interface can mislead the evaluation of energy transport by conduction, because it creates a uniform temperature layer just

under the interface where the temperature gradient is zero. They also observed that, at a certain low pressure threshold, thermocapillary flow starts creating turbulence and the evaporation flux suddenly increases.

In 2005, to quantify the energy transport by thermocapillary convection, Fei Duan and C. A. Ward [31] conducted an experimental analysis along with a theoretical prediction on the same evaporation condition with the funnel. The experiments were conducted under a pressure range of 250 Pa to 800 Pa, a vapour phase temperature range of -8 ℃ to 5℃ and water as the evaporating liquid. They calculated the Marangoni number by measuring the interfacial liquid velocity. In the prediction, they introduced a term called 'surface thermal capacity' where they considered that the energy transported by the thermocapillary flow is the energy carried along the surface. They concluded that, when the evaporation rate is high then the thermal conductivity of the water cannot supply enough energy, and this situation requires a higher Marangoni number to provide energy by thermocapillary convection.

In the same year, another experimental investigation was done by Duan and C.A. Ward [32] to confirm that the 'surface thermal capacity' is a property of the surface. This time, they observe the evaporation dynamics on a cylindrical surface which was 4.4 time larger than the spherical surface, but other measurement

apparatuses were the same. They used the same value for the 'surface thermal capacity' to predict the total energy transport for the cylindrical surface. They got agreement with the experimental results and confirmed that the 'surface thermal capacity' is a property of the evaporating surface.

In 2009, Fei Duan and Ward [33] conducted another experimental analysis to see the effect of liquid heating on the evaporation from a spherical interface. They used the same conical funnel mouth to create spherical interface. They maintained the throat temperature from 3.59℃ to 21.81 ℃ and vapour pressure was maintained around 600 Pa. They observed that the evaporation rate increases with the throat temperature. They concluded that, at low throat temperature the thermal conduction and the thermocapillary convection balance the rate of energy required for the evaporation. However, in case of high throat temperature, they found that the interfacial turbulence induced by the thermocapillary convection needs to be taken into account to explain the complete energy transport.

In 2010, H. Ghasemi and C.A. Ward [4] experimentally investigated the mechanisms of energy transport in an evaporating sessile droplet. Unlike the conical funnel used in most of their previous experiments, for this experiment a pinned steady sessile droplet was formed on top of a polished copper surface. Buoyancy driven flow was eliminated like other previous experiments, the vapour phase

temperature was maintained from 2℃ to 4.3 ℃ and the same miniature thermocouple of 25.4 μm diameter was used in the experiment. A spherical cap shape droplet of 9 mm base diameter was used for the experiment, using the measurements from this experiment, they predicted the evaporation dynamics of a spherical droplet which contains the cap of 9 mm diameter. They concluded that, the dominant mode of energy transport varies along the interface; at the apex, all the energy is transported to the interface through conduction, and near the three phase contact line thermocapillary convection is the larger mode of energy transport. They claimed that the thermocapillary convection can contribute as high as 98.4% of energy required for evaporation. Their work was done on a spherical cap with very low contact angle, but conclusions were made based on the spherical droplet predicted from the experimental data.

B. Sobac and D. Brutin worked on the energy transport mechanism to the interface. In 2012, B. Sobac and D. Brutin [34] experimentally observed thermal convective instabilities driven by evaporation in a drying ethanol droplet on a heated substrate, where substrate temperature was maintained from 30 to 60 ℃, ambient relative humidity was 40-50% and the pressure was atmospheric. They found that both the thermal conduction and the convection are responsible for the energy

transport to the interface. However, it was a spherical cap droplet and they did not quantify the contribution of these modes of energy transport.

In the same year, another study, B. Sobac and Brutin.[35], experimentally investigated the effect of substrate temperature and substrate properties on an evaporating pinned water droplet, for both hydrophilic and hydrophobic condition. In their experiment, the substrate temperature was maintained from 25 to 75℃ and the materials with different conductivities were used as the substrate. They found that with increase in the substrate temperature, energy transport mechanism related to temperature induced convection becomes increasingly important. In addition, they recommended to take buoyancy into consideration at high temperature situations. However, in this study they worked on both hydrophilic and hydrophobic conditions, but they did not work on the spherical droplet and the conclusion was based on the qualitative analysis.

2.4 A research gap in the field of evaporative cooling

In the hot surface cooling applications, such as microelectronics cooling applications, the surface temperature can be 50℃ to 70℃, pressure needs to be atmospheric, and the local surrounding temperature can be higher than the room temperature. In case of the evaporative cooling of air by the evaporation of water, the space air can be 35

to 45℃. Therefore, to implement the *cooling technology* based on the sessile droplet evaporation, these applications require a proper understanding of the energy transport mechanisms from the hot substrate to the interface of the evaporation, and the energy transport mechanism from the hot surrounding air to the interface. In addition, the evaporating droplet needs to be in spherical shape to apply established conduction equations for spherical coordinates. The research work on the interfacial energy transport [4, 9-11, 30-33] were done under ultra-low pressure experimental condition, and the vapour phase temperature was as low as 1.5℃ . It is not clear whether all the findings of these work are only valid for ultra-low pressure conditions. Some of this work [9, 11, 30-33] was done on the spherical shape interface (funnel), not on sessile droplets. The experimental investigation of the energy transport with the sessile droplet [4] was done under ultra-low pressure with very pure liquids and the droplet was not spherical. To the best of the author's knowledge there have been no experimental investigations on the interfacial energy transport mechanisms involved in the evaporation of a spherical shape sessile droplet under practical environmental conditions.

2.5 Objectives

The first objective of this research work is to determine energy transport and internal flow in an evaporating sessile droplet for practical conditions for evaporative cooling applications. All the experiments were conducted under atmospheric pressure which is the normal operating pressure for an evaporative cooling system. A millimetre sized spherical droplet on a copper substrate was investigated with practical substrate and ambient temperatures.

The first objective includes two steps, the first step is to measure the temperature profile of the interfacial vapour and liquid phases under practical substrate and ambient conditions, because these temperature profiles throughout the droplet surface provide information regarding the interfacial energy transport. The second step is to calculate the evaporation flux associated with thermal conduction along the droplet surface and the corresponding evaporation rate was calculated from the evaporation flux distribution. This evaporation rate can be compared with the actual evaporation measured experimentally to understand the relative contribution of conduction energy transport and other modes of energy transport. Since the conduction energy transport may not be the only mode of energy transport in some conditions, the surface temperature distribution of the droplet was used to figure out the direction of internal convection.

The second objective is to determine if there is a temperature discontinuity at the interface in practical conditions. The temperature discontinuity along the interface may be used as a tool to explain the evaporation dynamics and the interfacial energy transport.

Chapter 3

3 EXPERIMENTAL METHODS AND SETUP

It is described in the first chapter that the temperature profile of the bulk liquid phase can be used to calculate the rate of conduction energy transport to the interface and to determine the directions of the droplet internal flows. At the same time, the temperature profile of the vapour phase indicates energy transport through this surrounding medium to the interface. Therefore the experimental setup built for this experiment, is capable of measuring the liquid and vapour phase temperature accurately near the interface. In this chapter, the detailed experimental methods are described along with the experimental setup used for the observations.

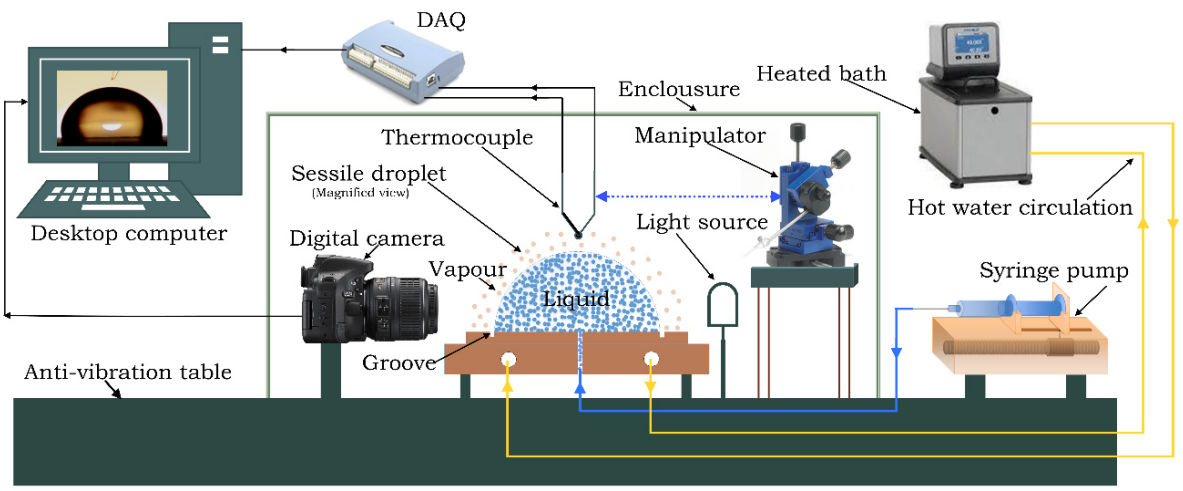

Figure 3.1 Schematic of the experimental setup.

3.1 Setup

The schematic diagram, shown in Figure 3.1, presents all the major apparatuses used in the experimental setup. An experimental setup was built with all these apparatuses, shown in Figure 3.2, and an enclosure was used to maintain steady thermal conditions surrounding the droplet, which is not shown in Figure 3.1. Temperature measurements were done in both the liquid and vapour phase with a T type miniature thermocouple with a bead of ~50 μm diameter, which is connected with the computer through the DAQ device. For proper positioning of the thermocouple, the interface was visualized with a digital camera (Camera body: *Nikon D5200* and Lens*: Nikon Af-s Dx Micro 40mm F2.8G*), which is connected with

the computer. Software was used to control the camera by the computer and droplet size was monitored throughout the experiment. The micro-lens enabled the camera to monitor the interface accurately. A light source behind the droplet, helps to detect the interface precisely. The heated bath maintained the isothermal condition of the droplet substrate by circulating hot liquid through it. The syringe pump maintained steady droplet shape by circulating a flow rate equal to the evaporation rate though the bottom of the sessile droplet. The groove, shown in Figure 3.1, was cut to create a spherical droplet on the copper substrate. Relative humidity inside the enclosure, was measured by a hygrometer, shown in Figure 3.2. The experimental setup was equipped with all the necessary apparatuses and the methods are described in section 3.3 of the current chapter.

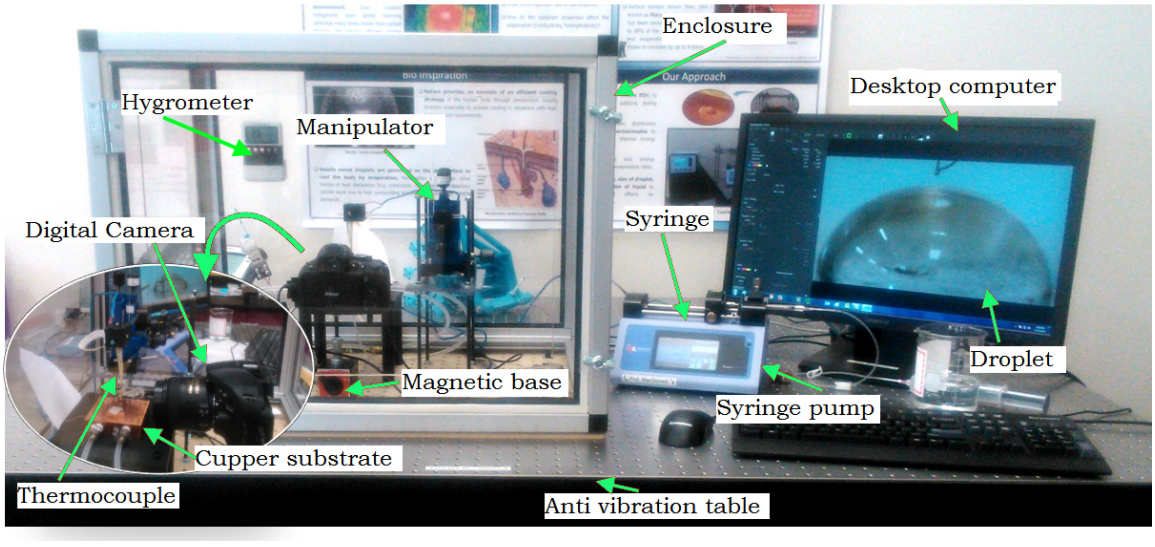

Figure 3.2 The experimental setup used in the '*MacDonald Lab*'.

3.2 Temperature measurement normal to the interface

It is explained in the introduction that, calculation of the local evaporation flux associated with the conduction requires the derivative of the vapour and liquid phase temperature at the interface, $\left(\frac{dT^V}{dr}\right)_{r=r_i}$ and $\left(\frac{dT^L}{dr}\right)_{r=r_i}$. These derivatives can be obtained from the vapour and liquid phase temperature profiles at the interface for different polar angle '∅'. The evaporation rate associated with conduction energy transport can be obtained from the local evaporation flux and this rate was compared with the actual evaporation rate 'J_{ev}'obtained from the syringe pump.

At six different angular position, ∅=0°, 30°, 45°, 60°, 70°and 80°", temperature of the liquid and vapour phases were measured with temperature sensor along the radial direction normal to the interface (Figure 3.3). Inside the liquid phase, temperature measurement of seven different points were done within 1.5 mm from the interface along the normal direction. Similarly, in the vapour phase, temperature measurement of seven different points were done within 3.0 mm from the interface. Only difference is, inside the liquid phase distance between two points were 0.25mm but in the vapour phase it was 0.5mm, because the liquid phase offers steady and stable measurement within shorter distance.

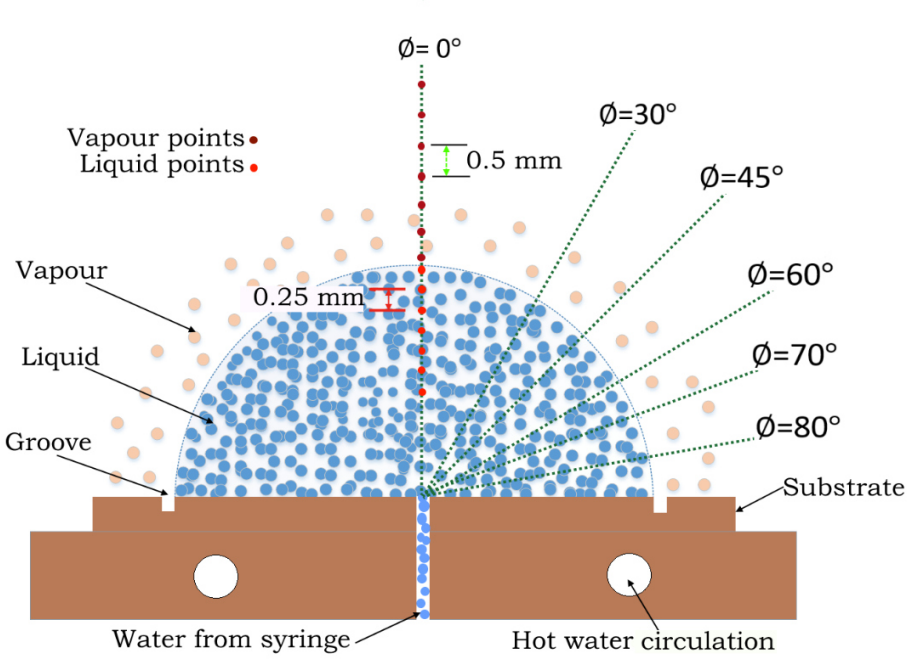

Figure 3.3 The temperature measurement procedure in different points inside the liquid and vapour phases.

The angle measurements and the temperature sensor positioning are done with the help of a digital camera, a desktop computer and a manipulator. The camera used for the visualization of the interface, is directly connected to the computer and hence the computer screen works as a magnified view of the droplet as seen in the Figure 3.2. A digital screen protractor was used on the computer screen to measure the angle accurately and to place the manipulator in the same angle. The movement of the thermocouple bead, used as the temperature sensor, was visualized in the monitor. The manipulator is capable of placing the thermocouple bead with 5 μm accuracy, which made the measurements reliable. All the temperature sensors used

in the setup, were connected to a data acquisition device (DAQ device). The DAQ was connected with the computer that displays the plots of all the measurements in progress. These plots also help to keep an eye on the enclosure temperature and substrate surface temperature along with the interface temperature. Therefore, the experimental facility with all these apparatus made the experimental approach reliable and helped to obtain accurate experimental data.

3.3 Methods

In this section, a description of all the methods used in the experiment will be provided. The experimental observation of the energy transport in an evaporating sessile droplet requires a number of facilities in the setup; such as the formation of a steady sessile droplet on a substrate, the temperature control of the substrate, the temperature control of the surrounding air, visualization of the droplet interface, positioning of the temperature sensor in the vapour and liquid phases and the data acquisition system. In addition, for the physical measurement at the micro-scale, the entire system needs to be isolated from ground vibrations. All these above mentioned facilities were incorporated in the experimental setup used during this research work.

3.3.1 Formation of the steady droplet on the substrate

The first phase of the experimental setup, was to build a mechanism of the steady droplet formation on a substrate. The goal of this research work is the experimental analysis of a sessile droplet, where the shape and size of the droplet needs to be constant throughout the experiment. To do so, distilled water was fed to a spherical sessile droplet of 5 mm diameter from its bottom, through a micro-channel machined in a pure copper substrate. To keep the droplet size constant throughout the experiment, a syringe pump was used to feed the liquid to the sessile droplet continuously, and was set to maintain a flow equal to the evaporation rate of the droplet. The syringe pump used in the setup, is capable of maintaining a flow as low as a few pico-liters per minute. This is how, the actual evaporation rate can be obtained from the syringe pump. This actual evaporation rate was compared with the calculated evaporation rate obtained from the temperature profiles of the liquid and vapour phases. A 5 ml syringe was capable of maintaining a uniform flow rate for approximately 20 hours with a flow rate of 4 μL/min.

3.3.2 Contact line pinning

When a sessile droplet evaporates on a surface, it reduces its volume in two steps. Primarily it reduces the contact angle gradually with time, then the three phase

contact line starts reducing its distance from the center of the droplet. So to keep the droplet shape and size steady, a certain flow rate equal to the evaporation rate of the droplet, needs to be maintained from the syringe pump. This method of maintaining three phase contact line at a certain distance is termed as contact line pinning. A change in the flow rate of the syringe pump, can change the base size of the droplet, but the droplet will still maintain the shape of a spherical cap. However, it is challenging to maintain the pinned contact line just by regulating the liquid flow rate from the syringe pump. During the experiment, it was observed that other than the flow rate, some other factors can affect the contact line distance from the center of the droplet. A gradual deposition along with the contact line, a change in the ambient temperature, a change in the ambient relative humidity and a change in the substrate surface temperature can change the pinning distance suddenly. To adjust this distance, the syringe pump flow rate can be altered, but it takes long time to reach the equilibrium. Whereas, a spherical sessile droplet was required for our experiment to analyze the experimental data using the established model of the spherical droplet.

3.3.3 Forced pining of the droplet to maintain spherical shape

To overcome the challenge associated with the contact line pinning a circular groove was machined around the three phase contact line of the droplet. The contact angle

of the distilled water on a copper surface is less than 90°, but the groove provides a discontinuity of the substrate surface and that is why the droplet contact line was forced to be pinned with the sharp edge of the groove. Under this situation a spherical cap shape sessile water droplet can be maintained by adjusting the liquid flow rate from the syringe pump. However, the same groove can help to maintain the spherical cap shape, because the main role of the groove is to pin the three phase contact line at the same position. A low liquid flow rate from the syringe will maintain spherical cape shape and a higher flow rate can maintain a contact angle larger than 90°.

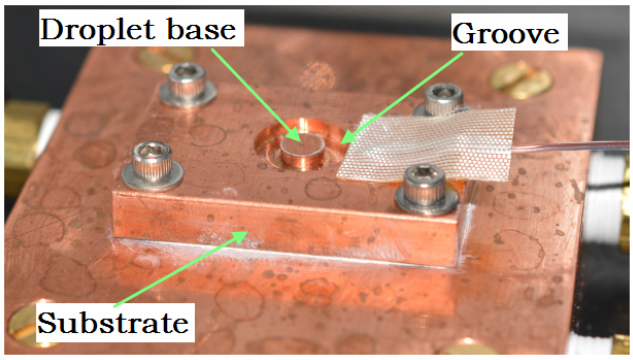

Figure 3.4 The groove on the copper substrate for forced pinning.

3.3.4 Substrate preparation

A metal base (3”x2.5”x0.75”) made of pure copper, is connected with a heated bath to maintain a constant temperature. This base is placed on top of a support made of plastic plate that provides the same level of surface as the anti-vibration tabletop. The substrate of the droplet made of 1.5”x1”x0.25” copper piece is placed on top of

that metal base. A micro-channel with an opening of 0.014" diameter just below the droplet, is machined through both substrate as we as metal base. This micro-channel is connected with the syringe pump through a tubing arrangement. Figure 3.3 shows the substrate with metal base and the flow through the micro-channel.

3.4 Temperature control

To match the ambient conditions with practical evaporative cooling systems, the setup was built with the provision of controlling substrate temperature as well as ambient temperature. Two through holes of 0.25" diameter, machined inside the metal base, are connected with the heated bath to control the temperature of the substrate.

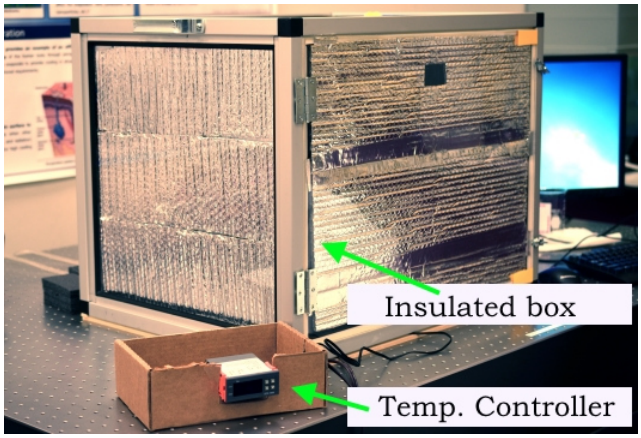

Figure 3.5 Insulated enclosure to maintain high ambient temperature.

To analyze the evaporation process under different ambient air condition, the temperature of the surrounding air needs to be maintained steady. To do so, an

artificial surrounding air was maintained by putting the entire experimental setup inside a box used as an enclosure, shown in Figure 3.5. The enclosure is made of aluminium frame and acrylic sheets. A heated lamp with the temperature controller was used to heat up the air of the enclosure when needed. The temperature controller can maintain a constant temperature inside the enclosure.

The reasons of building the enclosure are the unsteady air circulation inside the lab space and the unsteady lab space temperature. These factors affect the droplet ambient suddenly and it is difficult to control ambient conditions in this situation. In addition, light rays from different direction to the droplet affect the visualization of droplet contact line with camera. So light rays from different direction of the droplet, especially from the top were blocked. The enclosure solved the issue of unsteady ambient conditions.

The bottom side of the box was open and a door in the front side of the box facilitated the access inside the box. The tabletop is made of carbon steel and the conductive tabletop can change the inside temperature of the box. Therefore, the bottom side of the box was insulated with a wood board sheet. To maintain high ambient temperature, the inner sides of the box were insulated with high temperature insulation, shown in Figure 3.5. The temperature of the enclosure was recorded by the data acquisition device throughout the experiment.

3.5 Visualization of the interface

A proper visualization technique is essential to measure the temperature at different location of the liquid and vapour phases. The interface of the droplet was being monitored continuously by a digital camera connected with the computer, using its 'live view' mode. The interfacial region of the droplet was magnified in the computer screen and by activating its grid view, the droplet's size was being cross checked continuously.

Any kind of vibration in the droplet makes the interface of the droplet unstable. In this situation, it is difficult to track the interface and it incorporates unwanted noise in the temperature measurement. To eliminate this challenge, an anti-vibration tabletop is used as the base of the setup. This tabletop offers a level surface with the help of a compressor, dedicated for the table. It has ¼"-20 taped holes throughout the tabletop and these facilitate mounting of different apparatus. The visualization of the interface was done with good accuracy.

3.6 Measurement challenges

One of the measurement challenges was the condensation of moisture on the thermocouple in the vapour phase. During the measurement of the interfacial vapour phase temperature, the vapour can condensate on the bead of the thermocouple, if

it is placed too close to the interface, because vapour at that region is saturated. This kind of condensation makes the measurement of the temperature difficult at the vapour phase closer to the interface, because the condensation of the thermocouple quickly jumps on the interface and the thermocouple sticks on the droplet surface. This challenge was overcome by placing the thermocouple at a safe distance of around $50\mu m$ from the interface.

It is challenging to measure temperature along the interfacial region. The temperature sensor requires precise positioning and it should be able to provide significant measurement with micro-scale movement. For this experimental setup a T-type thermocouple with 50 μm bead was used which is capable of measuring temperature with an accuracy of $\pm$ 0.5℃. The manipulator used for proper positioning of the thermocouple bead, can make precise movement as low as $5\mu m$, in the experiment an additional scale was added with the knob of the manipulator that helps to move precisely as low as $7\mu m$. The anti-vibration table can eliminate greater than 96% of the ground vibration, and it helps to eliminate the noise in the temperature measurement associated with the ground vibration. The digital camera used in the setup enabled a clear visualization of $5\sim 10\mu m$ at the interfacial region, which is enough for the accurate positioning of thermocouple. Another crucial measurement of these experiments is the measurement of actual evaporation rate

from the syringe pump, they syringe pump used in the setup is capable of maintaining a flow rate as low as 1.28 pL/min with ± 0.5% accuracy. The heated bath used to maintain isothermal substrate temperature is capable of maintaining temperature with an accuracy of ±0.01C, and the enclosure temperature was maintained with an accuracy of ±0.5℃ using the temperature regulator and heated lamp.

Therefore, all the apparatuses used in this setup, offer high accuracy and precision which is essential for micro-scale measurements. The experimental data obtained from the setup should be reliable to explain the evaporation dynamics at the interface.

Chapter 4

4 RESULT AND DISCUSSION

The experimental method described in the previous chapter, was used to measure the temperature profile of the vapour and liquid phases of the evaporating droplet. Four sets of experiment were conducted with a spherical droplet at different temperatures of the substrate and the ambient air, to match the experimental conditions with the operating conditions of the practical applications: Case (I): high substrate temperature and low ambient temperature, Case (II): high substrate temperature and high ambient temperature, Case (III): similar substrate temperature and ambient temperature and Case (IV): low substrate temperature and high ambient temperature. In practical applications, such as microelectronic device cooling and evaporative air cooling, a temperature of 60℃ is considered as a high substrate temperature and a temperature of 40℃ is considered to be a high ambient temperature. Details of the experimental conditions are summarized in the Table 4.1.

Table 4.1 Summary of the experimental environments for four different cases.

	Case-I	Case-II	Case-III	Case-IV
Substrate temperature	60℃	60℃	32℃	29.5℃
Enclosure temperature	30℃	40℃	29℃	40℃
Enclosure pressure	1 atm	1 atm	1 atm	1 atm
Substrate material	Cu	Cu	Cu	Cu
Liquid	Water	Water	Water	Water
Droplet diameter	5 mm	5 mm	5 mm	5 mm

In every set of experiments, the same distilled water was used as the liquid of the droplet and a small size droplet of 5 mm diameter was maintained throughout the experiments to reduce the effect of buoyancy force and the shape of the droplet was maintained spherical. The relative humidity of the enclosure was approximately 30% throughout the experiments.

The temperature profiles of the liquid and vapour phases along the interface were measured for all above mentioned cases following the experimental method mentioned in the previous chapter. The local evaporation fluxes and corresponding evaporation rate associated with the conduction energy transport were calculated from the temperature profiles using equations (1) and (2) respectively mentioned in section 1.4.3. This evaporation rate was compared with the actual evaporation rate obtained from the syringe pump, J_{actual} to calculate the relative contribution of

conduction energy transport for all the cases. The temperature discontinuities along the interfaces were determined from the interfacial temperature profiles of the liquid and vapour phases. In addition, the directions of internal convections were determined from the droplet surface temperature distribution.

In the next few sections, the analysis of the obtained data from all four set of experiment will be discussed with the help of corresponding plots.

4.1 Case (I) - High substrate temperature and low ambient temperature.

In this case, the temperature of the substrate was maintained at 60℃, the ambient temperature was maintained at 30℃ and the entire experiment was conducted under atmospheric pressure. In this phase of the research, the modes of interfacial energy transport during the evaporation of a sessile droplet at high substrate temperature and low ambient temperature were experimentally observed.

4.1.1 Temperature profile in the liquid and the vapour phases Case (I)

For the current experimental condition, the temperature profiles of both the liquid and the vapour phases are plotted at two sides of the interface in Figures 4.1 to 4.6 for ∅= 0°, 30°, 45°, 60°, 70° and 80° respectively. For each data point 60 temperature measurements were recorded in a minute under steady state conditions with one

second interval, then the average of those measurements were taken as the temperature at that particular point. The error bars were calculated by standard deviation ($\pm\sigma$) of the sample of 60 measurements. Since the droplet radius was 2.5 mm, a line indicating the interface was drawn at r =2.5 mm. The distance of different measurement points were calculated from the interface, therefore a small variation of the interface location will not affect the temperature profile of the liquid and the vapor phases along the interface. The data points at the liquid phase were fitted with a second order polynomial of r, $T^L = A_0 + A_1 r + A_2 r^2$, here A_0, A_1 and A_2 are constants; and the data points at the vapour phase were fitted with an inverse first order polynomial of r, $T^V = A_0 + \frac{B_0}{r}$, here A_0 and B_0 are some constant. Both polynomials are solutions to the energy equation in spherical coordinates with the appropriate boundary conditions. At each position, the liquid phase transports energy to the interface which is apparent from the negative slopes of its temperature profiles at the interface. However, the vapour phase transports energy to the interface near three phase contact line, shown in Figure 4.6, but it takes energy from the interface in the rest of the position, shown in Figure 4.1 to 4.5. From the plots it is evident, because the slope of the temperature profile at the interface is positive for $\emptyset$=80° and negative in all other positions.

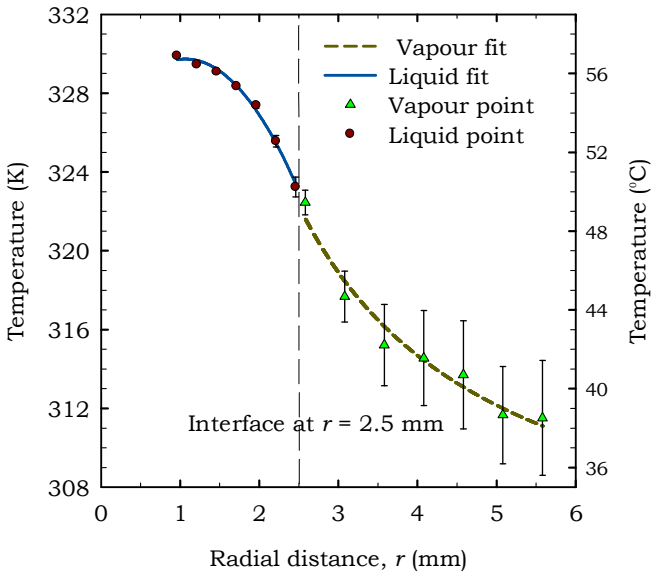

Figure 4.1 The liquid and vapour temperature profile at $\emptyset = 0°$ (Case-I).

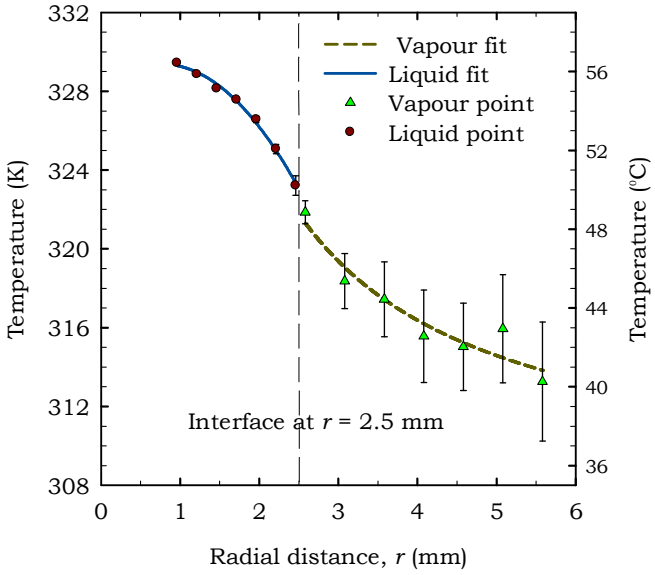

Figure 4.2 The liquid and vapour temperature profile at $\emptyset = 30°$ (Case-I).

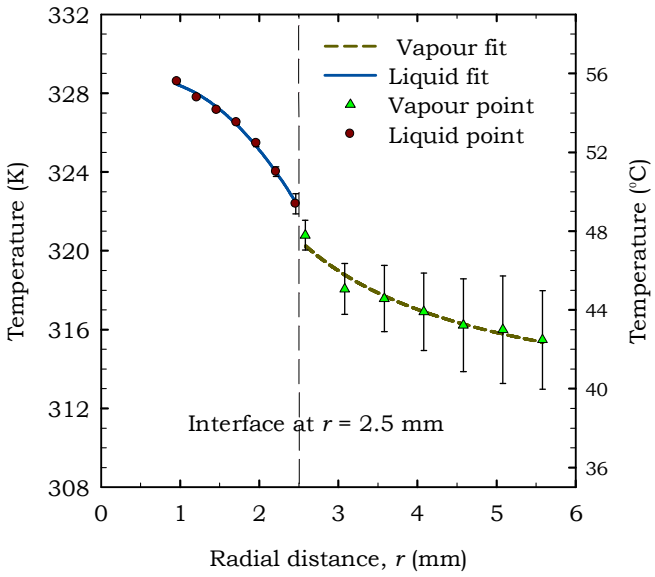

Figure 4.3 The liquid and vapour temperature profile at $\emptyset = 45°$ (Case-I).

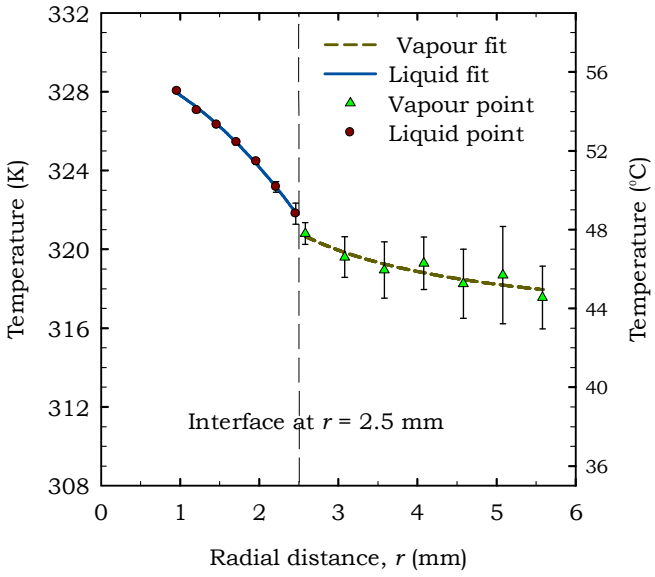

Figure 4.4 The liquid and vapour temperature profile at $\emptyset = 60°$ (Case-I).

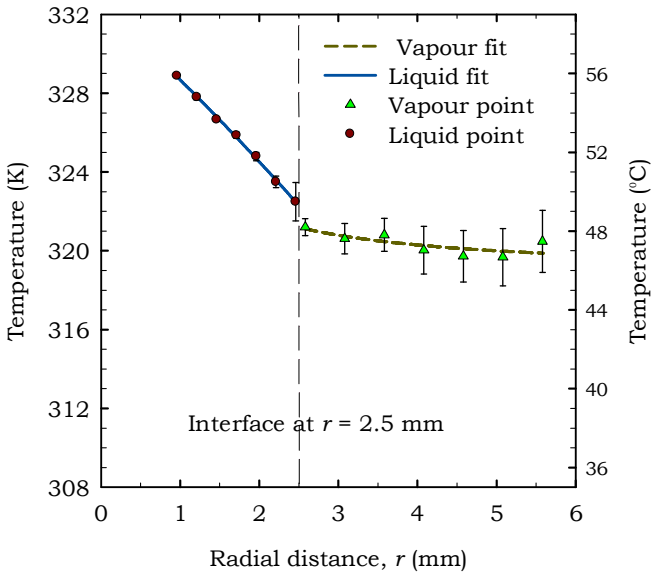

Figure 4.5 The liquid and vapour temperature profile at $\emptyset = 70°$ (Case-I).

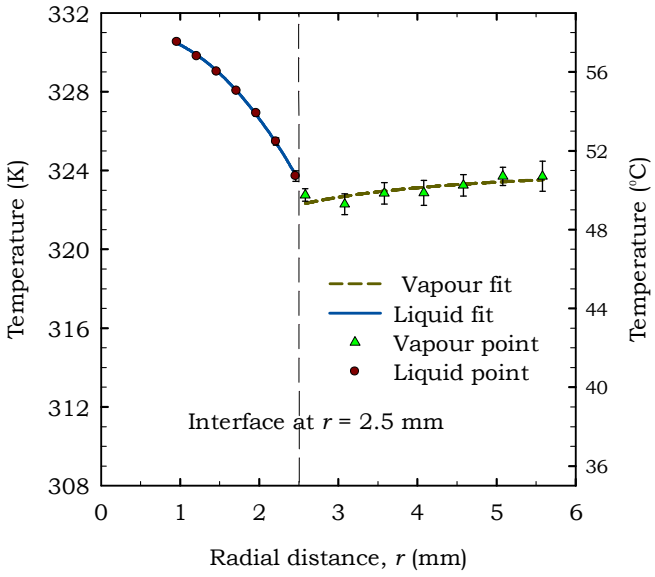

Figure 4.6 The liquid and vapour temperature profile at $\emptyset = 80°$ (Case-I).

This change can be understood because near the three phase contact line, the vapour phase surrounding the droplet gets heated up by the hot substrate and maintains a high temperature, but for rest of the droplet surface, the vapour phase maintains a low temperature due to the low temperature of the ambient air.

As it is mentioned in the introduction, the difference between the temperature of the liquid phase and the vapour phase is termed as the temperature discontinuity. Figures 4.1 to 4.6, show that at the interface there is a discontinuity in the temperature of the liquid phase and the vapour phase. A temperature discontinuity of 1℃ to 2.5 ℃ were observed at different position of the droplet. A large temperature discontinuity at the interface can influence the evaporation process.

4.1.2 Contribution of the liquid and the vapour phases in the conduction energy transport -Case (I).

As it is mentioned in the introduction, the contribution of the liquid and the vapour phases in the conduction energy transport to the interface was calculated from the derivatives of their temperature profiles at interface, shown in Figures 4.1 to 4.6, where the rate of energy conducted through the liquid phase is $k_L \left(\frac{dT^L}{dr}\right)_{r=r_i}$ and the rate of energy conducted through the vapour phase is $k_V \left(\frac{dT^V}{dr}\right)_{r=r_i}$. Figure 4.7 shows the comparative contribution of the vapour and the liquid phases at different position

of the droplet. The liquid phase curve shows that, the rate of energy conducted from the liquid phase doesn't follow a uniform increasing or decreasing trend from the droplet apex to the three phase contact line along with the interface.

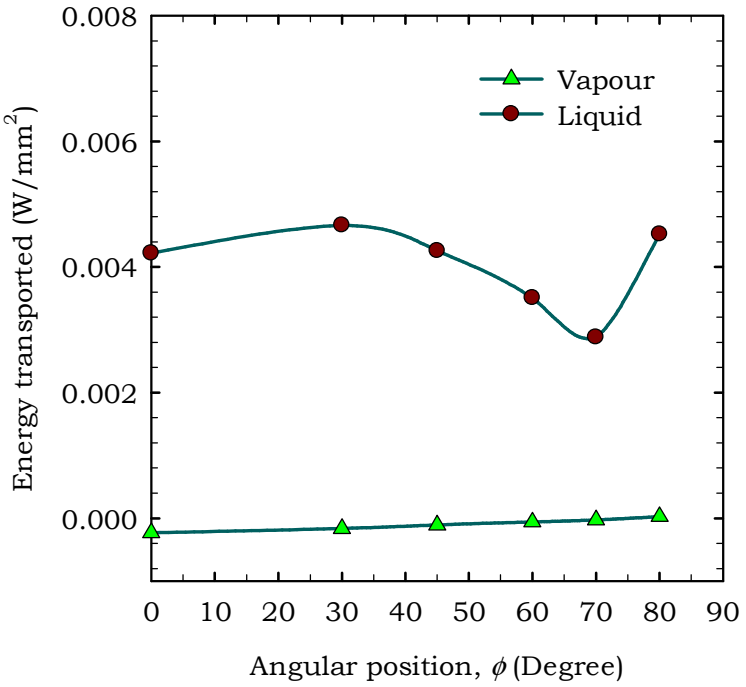

Figure 4.7 Contribution of the liquid and the vapour phases in conduction energy transport (Case-I).

Figure 4.7 shows that between ∅=0° and ∅=30° this rate is high but there is no drastic increase or decrease in the value. It is very significant that, between ∅=60° and ∅=90° there is a drastic increase in that rate, because it show that its value increases near the three phase contact line. A gradual decrease in that rate is observed between ∅=30° and ∅=70°, where it is minimum at ∅=70°, that trend

indicates the probable droplet internal flows that affect the conduction through the liquid phase in this region. The vapour phase curve shows that from ∅=0° to ∅=70°, its contribution is negative, which indicates it takes energy from the interface in this region; and between ∅=70° and ∅=90°, it transports energy to the interface as the contribution is positive, shown in Figure 4.7. However, in each angular position, the rate of energy conducted through the vapour phase (negative or positive contribution) is very low compared to the rate of energy conducted through the liquid phase, because the thermal conductivity of the vapour is very low compared to the water.

4.1.3 The evaporation rate associated with the conduction energy transport- Case (I)

In this case, the total evaporation rate associated with the conduction energy transport to the interface depends on the conduction energy transport through the liquid phase, because from Figure 4.7 it is evident that the conduction energy transport through the vapour phase is insignificant compared to the conduction energy transport through the liquid phase. Using Equation (1) mentioned in the introduction, the local evaporation fluxes associated with the conduction energy transport, j_{ev} were calculated for all six angular position (∅= 0°, 30°, 45°, 60°, 70° and 80°). These local evaporations fluxes were plotted in Figure 4.8, the data points

of the local evaporation flux were fitted with a third order polynomial of "cos∅", which is $j_{ev}(\emptyset)$= 0.2173-0.8466 $\cos(\emptyset)$+1.5676$cos^2(\emptyset)$-0.8385$cos^3(\emptyset)$ for Case (I). Using Equation (2) mentioned in the introduction, the total evaporation rate associated with the conduction energy transport $'J_{ev}'$, was calculated by integrating that polynomial from ∅= 0° to ∅= 90°.

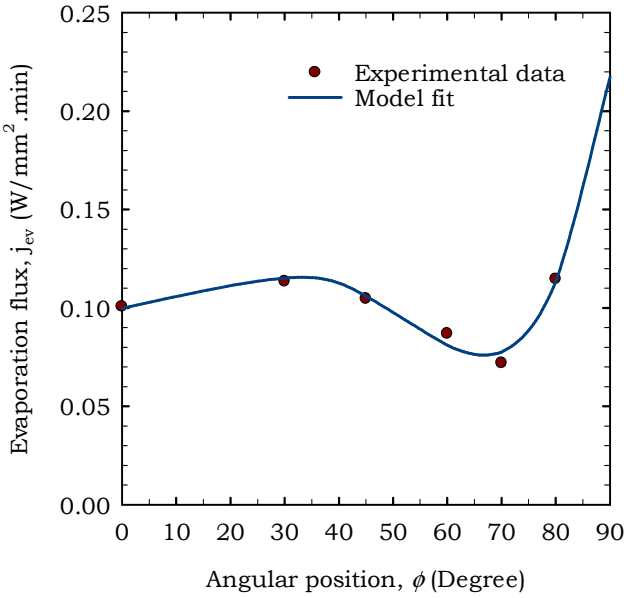

Figure 4.8 The local evaporation flux distribution from the apex to the three phase contact line (Case-I).

The figure 4.8 shows the local evaporation flux along at different positions and the estimated fitting. Similar to the energy contribution curve of the liquid phase plotted in Figure 4.7, the polynomial fitting of the local evaporation flux doesn't follow a uniform increasing or decreasing trend along the droplet surface. It follows similar trend of energy contribution curve of the liquid phase. So in this case, the energy

conducted through the liquid phase will determine the local evaporation flux. However, from the Figure 4.8 it is evident that the local evaporation flux near three phase contact line is higher than other region of the droplet. In this case, total evaporation rate associated with the conduction energy transport $'J_{ev}'$ was calculated as 4.19 μL/min. This total evaporation rate was compared with the actual evaporation rate, J_{actual}, obtained from the syringe pump, which was 4.6 μL/min. Since two evaporation rates are similar, in this case, the conduction energy transport to the interface is providing the required rate of energy supply for the evaporation. Therefore evaporation of a millimeter size spherical droplet on high temperature substrate and low temperature ambient, is dominated by the conduction energy transport through the liquid and the vapour phases.

4.1.4 Internal convective flows of the droplet - Case (I)

To analyze the convective flows in the droplet, the droplet surface temperatures were measured at all six angular position (∅= 0°, 30°, 45°, 60°, 70° and 80°). The gradient in the temperature distribution $\left(\frac{dT^L}{d\emptyset}\right)_{r=r_i}$, from the droplet apex to the three phase contact line, indicates the directions of the internal convective flows. Figure 4.9 shows the temperature distribution of the interfacial liquid phase along the droplet surface.

From the trend of the plot it is apparent that, the droplet apex (∅=0°) is colder than droplet bottom (∅=90°) which will cause buoyancy driven flow inside the droplet. The colder and heavy liquid from the apex tends to move towards the bottom; and the warmer and light liquid from the droplet bottom tends to move to the apex, this is how buoyancy driven flow can make convective flow inside the droplet shown in Figure 4.10.

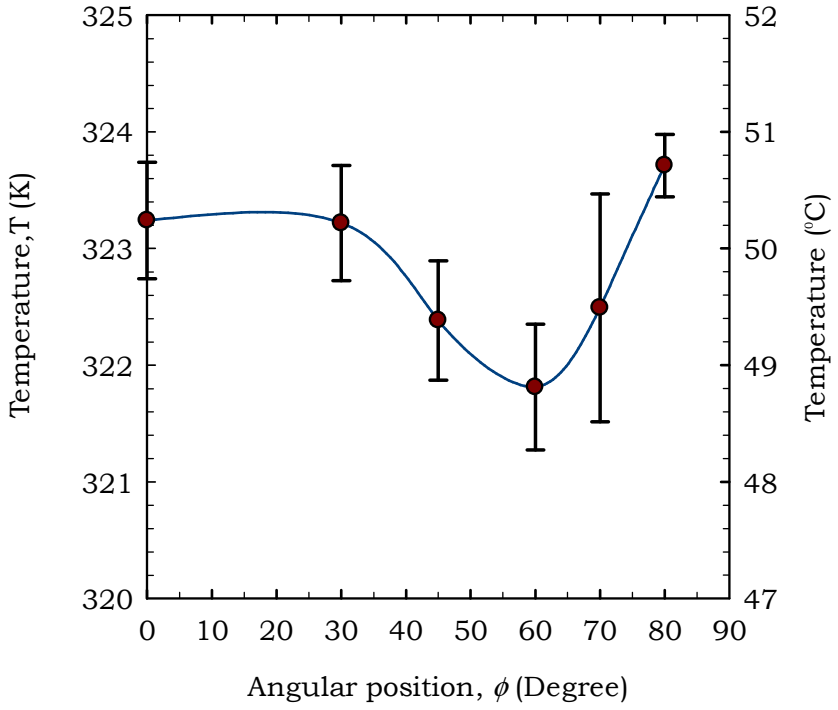

Figure 4.9 Surface temperature distribution from the apex to the three phase contact line (Case-I).

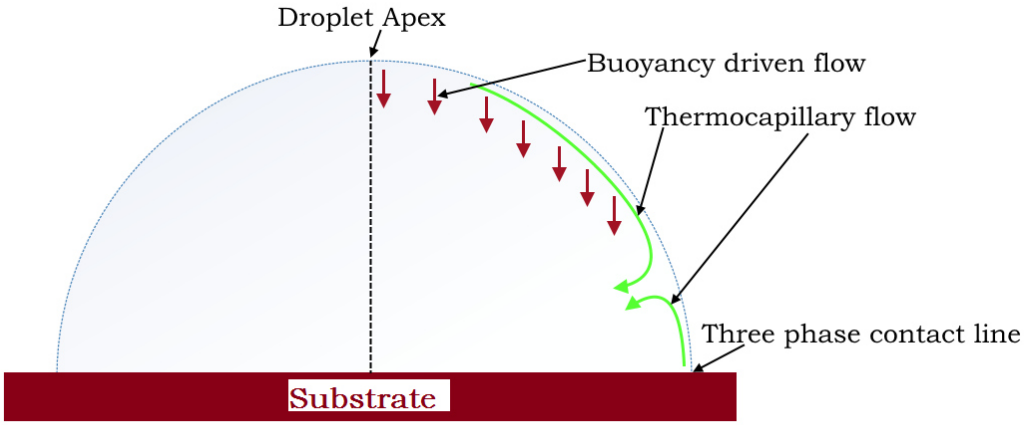

Figure 4.10 Estimated directions of the internal convection (Case-I, II and IV).

From the Figure 4.9, it is clear that droplet surface temperature at (∅=60°) is the minimum whereas both the apex temperature and the bottom temperature is higher than this region. This temperature gradient at the surface will create two different cell of thermocapillary flows directed opposite to each other as shown in Figure 4.10.The thermocapillary flow directed from the apex to the coldest point (∅=60°), will augment the buoyancy driven convection and the thermocapillary from directed from the three phase contact line to the coldest point, will oppose the buoyancy driven convection. These two convective flows meets at (∅=60°) and reduce the energy transport to the interface, shown in Figure 4.10.

4.2 Case (II) - High substrate temperature and high ambient temperature.

In this case, the temperature of the substrate was maintained at 60℃ just like the case (I), however the ambient temperature was increased to 40℃ and maintained throughout the experiment. Like all other experiments this experiment was conducted at atmospheric pressure. All the physical phenomena analyzed and discussed in case (I) were also analyzed here for Case (II).

4.2.1 Temperature profile in the liquid and the vapour phases- Case (II)

Similar to Case (I), the temperature profiles of both the liquid and the vapour phases are plotted at both sides of the interface in Figures 4.11 to 4.16 for $\emptyset = 0°$, 30°, 45°, 60°, 70° and 80° respectively. The temperature profile of the liquid phase shows a similar pattern to Case (I), where the liquid phase transports energy to the interface. However, the temperature profile of the vapour phase shows a different pattern than case (I), Figures 4.11 to 4.13 show that the slopes of the temperature profiles in $0° \leq \emptyset < 60°$ is negative, which indicate that in this region the vapour phase takes energy from the interface. In rest of the region, $60° \leq \emptyset \leq 90°$, the slopes of the temperature profiles is positive, shown in Figures 4.14 to 4.16.

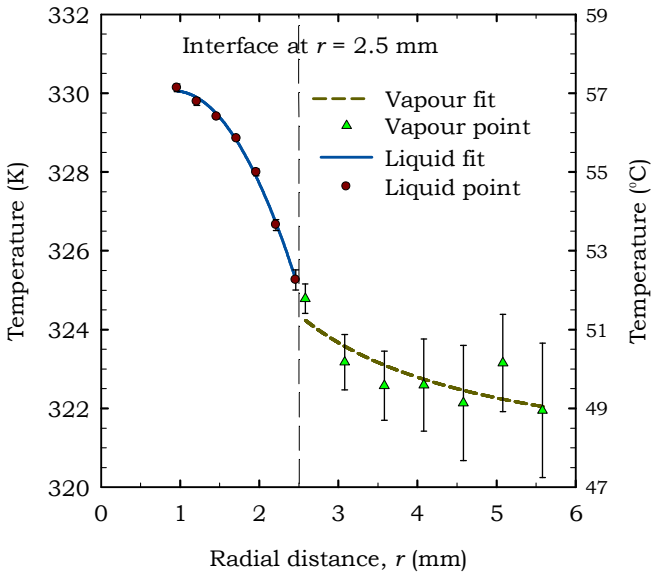

Figure 4.11 The liquid and vapour temperature profile at $\emptyset = 0°$ (Case-II).

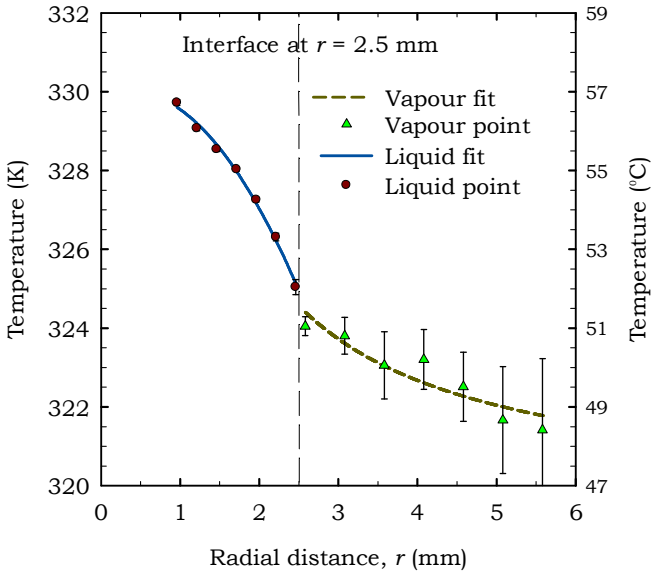

Figure 4.12 The liquid and vapour temperature profile at $\emptyset = 30°$ (Case-II).

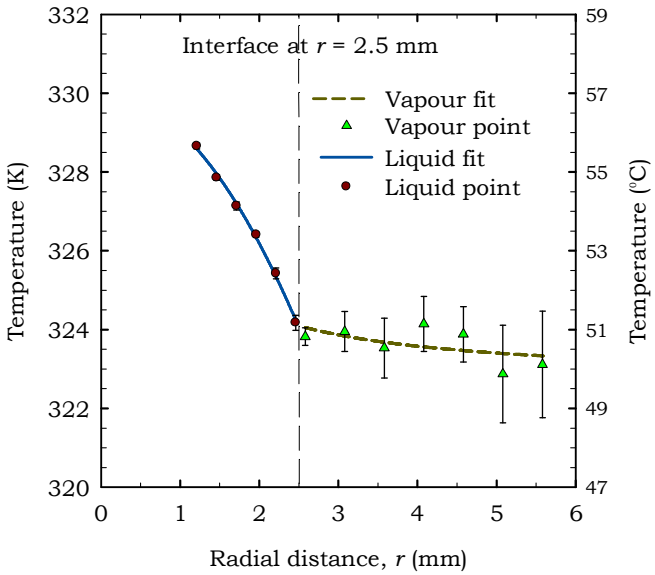

Figure 4.13 The liquid and vapour temperature profile at $\emptyset = 45°$ (Case-II).

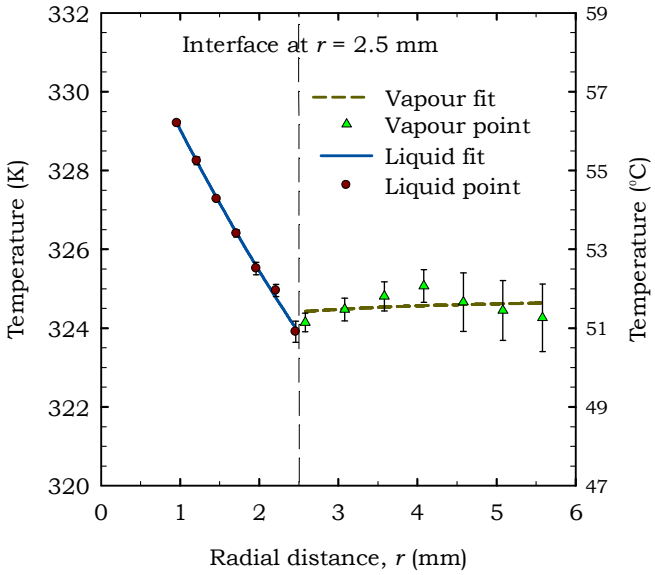

Figure 4.14 The liquid and vapour temperature profile at $\emptyset = 60°$ (Case-II).

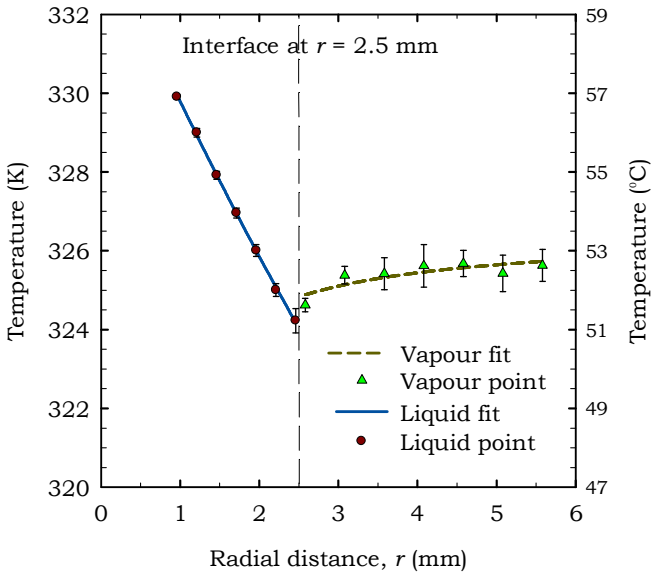

Figure 4.15 The liquid and vapour temperature profile at $\emptyset = 70°$ (Case-II).

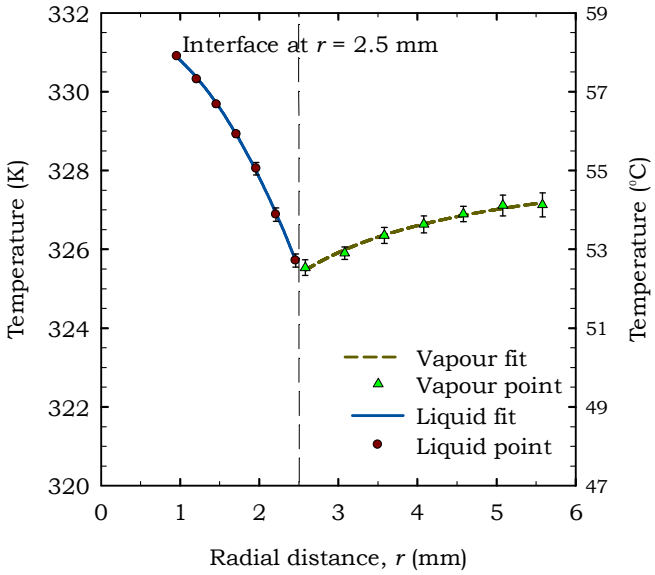

Figure 4.16 The liquid and vapour temperature profile at $\emptyset = 80°$ (Case-II).

Figures 4.14 to 4.16 indicate that in this region the vapour phase contributes energy to the interface. The change in slope from negative to positive near the bottom of the droplet indicates that, in this region the vapour phase surrounding the droplet gets heated up by the hot substrate like case (I). Therefore, it is evident that the hot substrate does not affect only the liquid phase of the droplet, it also affects the vapour phase surrounding the droplet.

In this case, temperature discontinuities were observed in Figures 4.11 to 4.16. Unlike case (I), in this case the maximum temperature jump was approximately 1℃ at ∅= 70°, however, the interfacial vapour phase temperature was higher than the interfacial liquid temperature at ∅= 70° which can affect the local evaporation flux.

4.2.2 Contribution of the liquid and the vapour phases in the conduction energy transport Case (II)

Figure 4.17 shows the comparative contribution of the vapour and the liquid phases at different position of the droplet. Unlike the case (I), at the apex, the conduction energy transport through the liquid phase is higher. This value decreased until ∅=60° where a sudden increase starts after this point, but in case (I) there was a decrease

from ∅=30° to ∅=70°. In the case (I) this lowest point was at ∅=70° but, in this case the lowest contribution from the liquid phase shifts to ∅=60°.

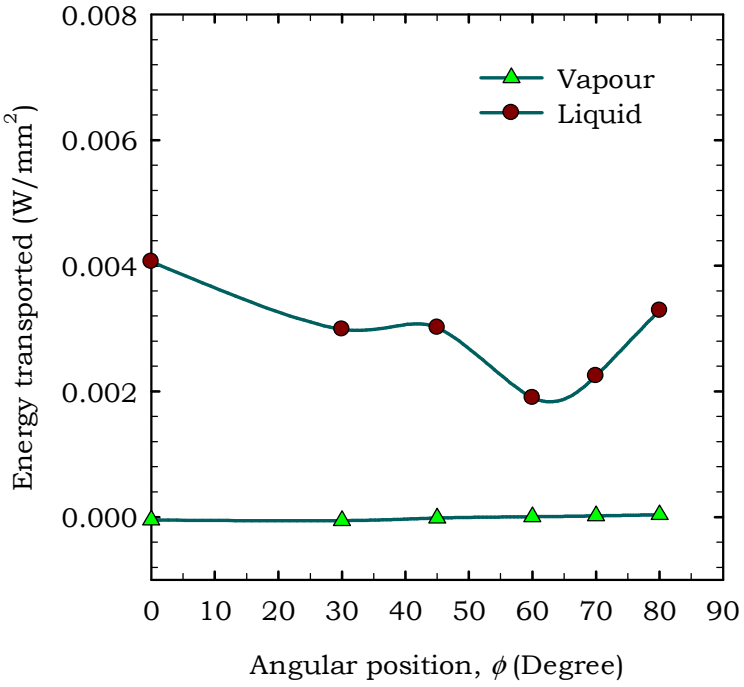

Figure 4.17 Contribution of the liquid and the vapour phases in conduction energy transport (Case-II).

The vapour phase curve shows that from ∅=0° to ∅=45°, its contribution is negative, which indicates it takes energy from the interface in this region; and between ∅=60° and ∅=90°, it transports energy to the interface as the contribution is positive. However, like case (I) in this case the rate of energy conducted through the vapour phase (negative or positive contribution) is negligible compared to the rate of energy conducted through the liquid phase.

4.2.3 The evaporation rate associated with the conduction energy transport -Case (II)

From Case (I), it is evident that the total evaporation rate associated with the conduction energy transport to the interface depends on the conduction energy transport through the liquid phase. Since in case (II) the substrate temperature is equally hot, in this case the conduction energy transport through the liquid also decides the evaporation flux. Figure 4.18 shows the local evaporation flux at different positions, the data points were fitted with a third order polynomial of "cos$\emptyset$", which is $j_{ev}(\emptyset)$= 0.1415-0.4393 $\cos(\emptyset)$+0.6475$cos^2(\emptyset)$-0.2515$cos^3(\emptyset)$ for Case (II).

Unlike Case (I), the local evaporation flux at $\emptyset$=80° is lower than the evaporation flux at the apex of the droplet. However, the local evaporation flux near three phase contact line is still higher than other region of the droplet. In this case, total evaporation rate associated with the conduction energy transport $'J_{ev}'$ was calculated as 2.93 µL/min and the actual evaporation rate obtained from the syringe pump was 4.35 µL/min. Unlike Case (I), in this case the evaporation rate associated with the conduction energy transport is only 67% of the actual evaporation rate. So we can conclude that when a spherical sessile droplet evaporates on a high temperature substrate, the contribution of the conduction energy transport decreases with the increase in the ambient temperature.

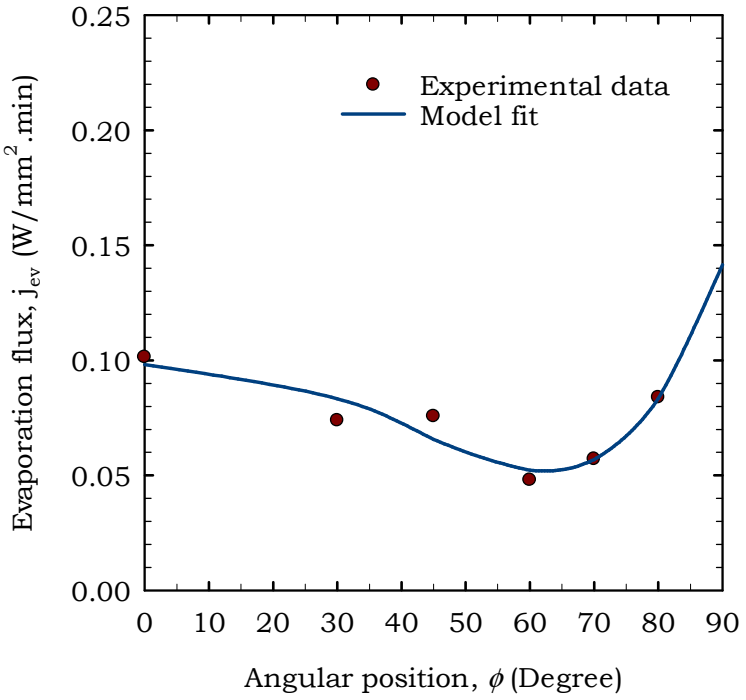

Figure 4.18 The local evaporation flux distribution from the apex to the three phase contact line (Case-II).

In addition, the total evaporation rate decreases from 4.6 to 4.35 μL/min, which indicates that in case of high temperature substrate, increase in ambient temperature decreases the evaporation rate. Therefore, in this kind of practical condition, with the increase in the ambient temperature the conduction energy transport becomes less dominant and it is possible that other modes of the energy transport become more dominant, including the convective internal flows.

4.2.4 Internal convective flows of the droplet -Case (II)

Figure 4.19 shows the temperature distribution of the interfacial liquid phase along the droplet surface. This temperature distribution plot shows a similar pattern to Case (I). In this case, like Case (I), the apex of the droplet (∅=0°) will also be colder than droplet bottom (∅=90°) which can be predicted from the trend of the plot. A similar buoyancy driven flow and two thermocapillary flows will form inside the droplet, shown in Figure 4.10.

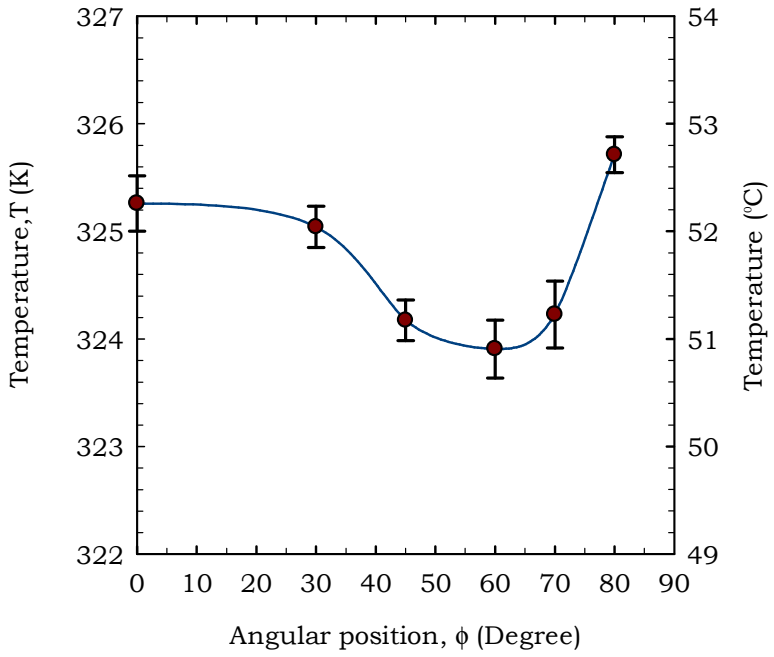

Figure 4.19 Surface temperature distribution from the apex to the three phase contact line (Case-II).

4.3 Case (III) - Similar substrate and ambient temperature.

In this case, the temperature of the substrate was maintained at 32℃ and the ambient temperature was maintained 29℃, throughout the experiment. This case is similar to Case (I), but the difference is that the substrate temperature is also low. The experiment was conducted under atmospheric pressure. All the physical phenomena analyzed and discussed in Case (I) were also analyzed in this case. The main purpose of choosing this set of temperatures for the substrate and the ambient is to observe the energy transport mechanism in the spherical droplet when both substrate and the ambient temperatures are similar

4.3.1 Temperature profile in the liquid and the vapour phases -Case (III)

In this case, like all other cases, the temperature profiles of both the liquid and the vapour phases are plotted at both sides of the interface in Figures 4.20 to 4.25 for ∅= 0°, 30°, 45°, 60°, 70° and 80° respectively. The temperature profile of the liquid phase shows similar pattern like case (I), where the liquid phase transports energy to the interface. However, the temperature profile of the vapour phase shows a different pattern than Case (I) and (II). In this case, like the liquid phase, the vapour phases also transport energy to the interface throughout the surface of the droplet.

Since the substrate temperature and the ambient temperature are low, the slopes of the temperature profile of the liquid phase and the vapour phase are low compared to Case (I) and (II). However, the slopes for the liquid phases are larger than the vapour phases.

Another, important observation is that, in this case near the three phase contact line, the substrate does not affect the temperature profile of the vapour phase, because of the similar temperature of the substrate and the ambient. Figures 4.20 to 4.25 show that, there are discontinuities in the temperature of the interfacial liquid phase and the interfacial vapour phase, but these temperature jumps are not equal at every position of the droplet surface. Near the droplet apex and the three phase contact line, the temperature jump is as high as 0.5℃ but in the middle region it is negligible. However, it is clear from the plots that near the apex, the interfacial vapour phase temperature is higher than the interfacial liquid temperature, but near the three phase contact line the interfacial vapour temperature is lower than the interfacial liquid temperature. This kind of variable temperature jump at the interface can affect the total evaporation rate significantly.

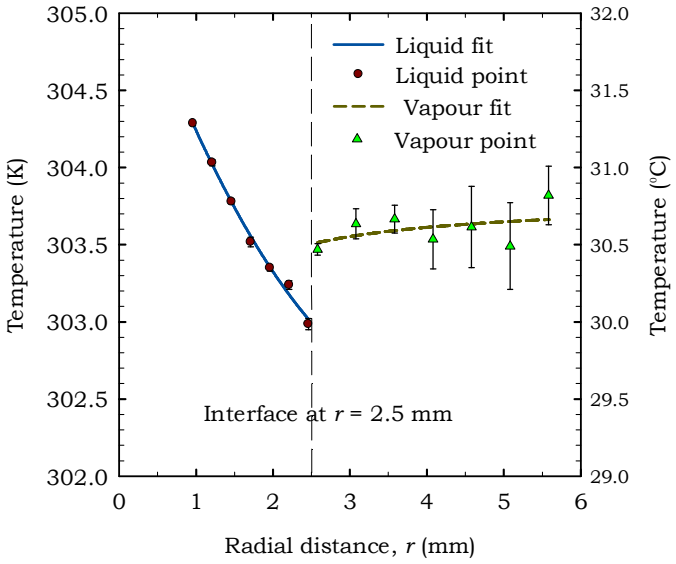

Figure 4.20 The liquid and vapour temperature profile at $\emptyset = 0°$ (Case-III).

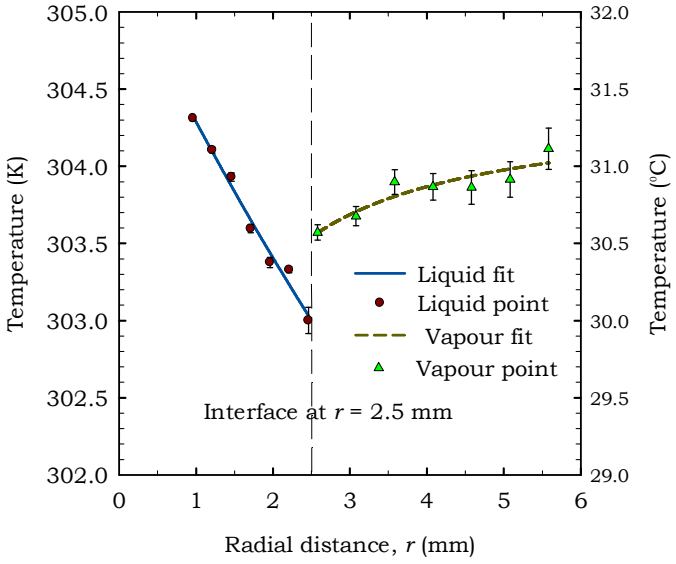

Figure 4.21 The liquid and vapour temperature profile at $\emptyset = 30°$ (Case-III).

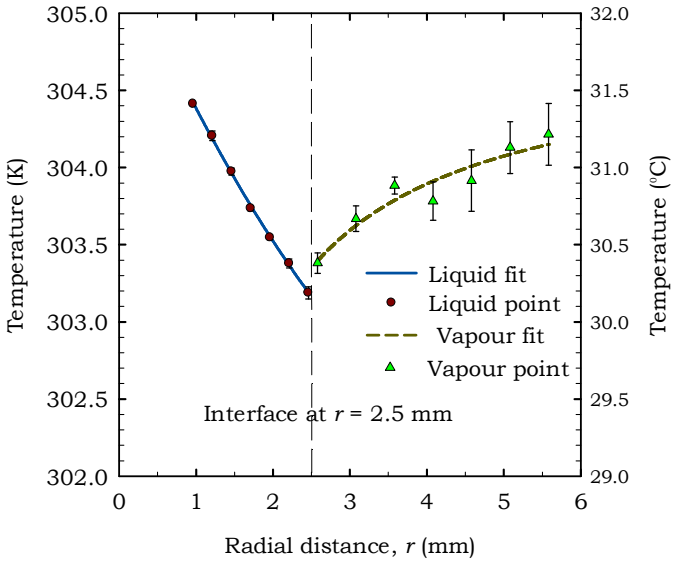

Figure 4.22 The liquid and vapour temperature profile at $\emptyset = 45°$ (Case-III).

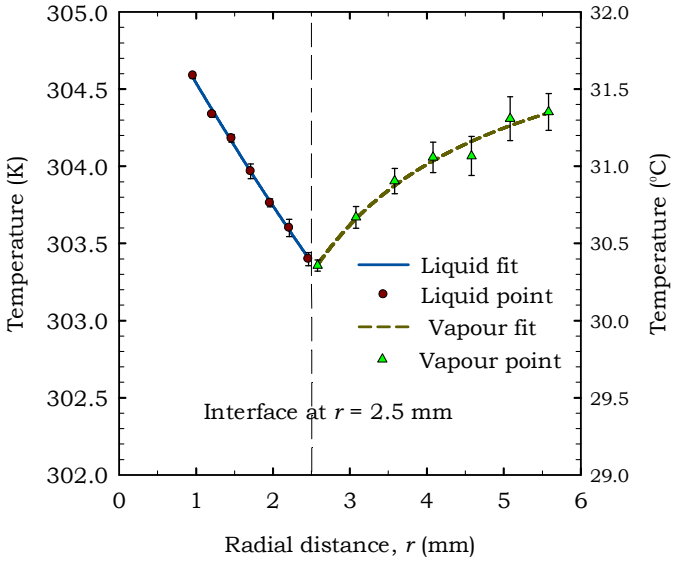

Figure 4.23 The liquid and vapour temperature profile at $\emptyset = 60°$ (Case-III).

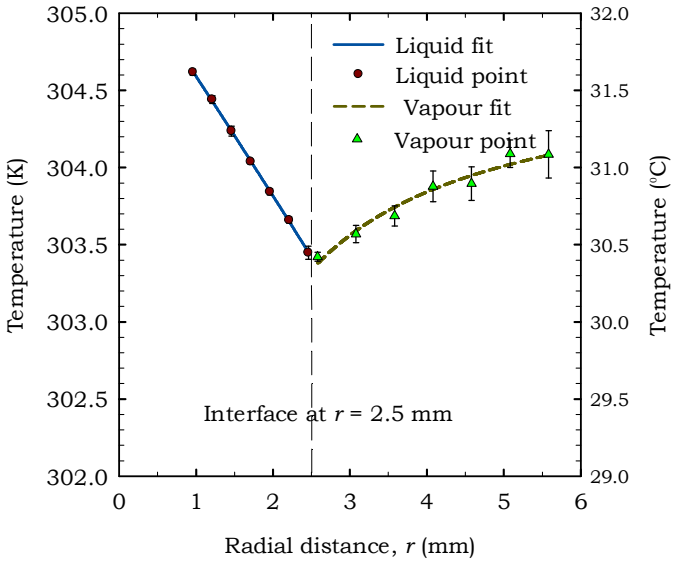

Figure 4.24 The liquid and vapour temperature profile at $\emptyset = 70°$ (Case-III).

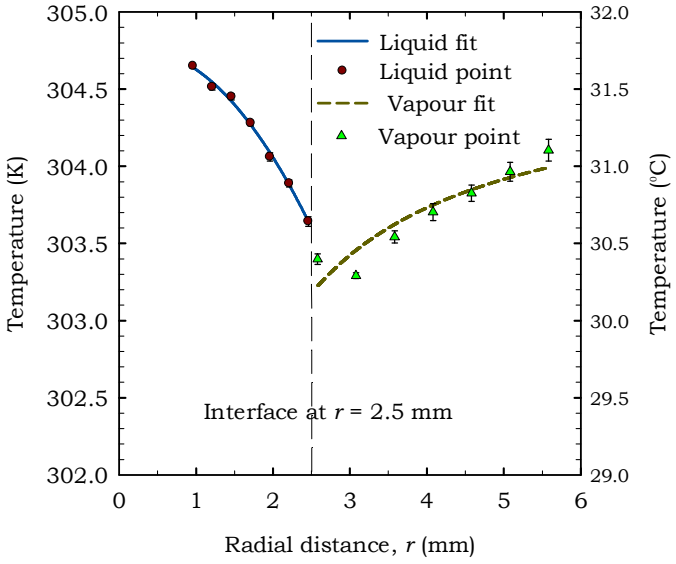

Figure 4.25 The liquid and vapour temperature profile at $\emptyset = 80°$ (Case-III).

4.3.2 Contribution of the liquid and the vapour phases in the conduction energy transport -Case (III)

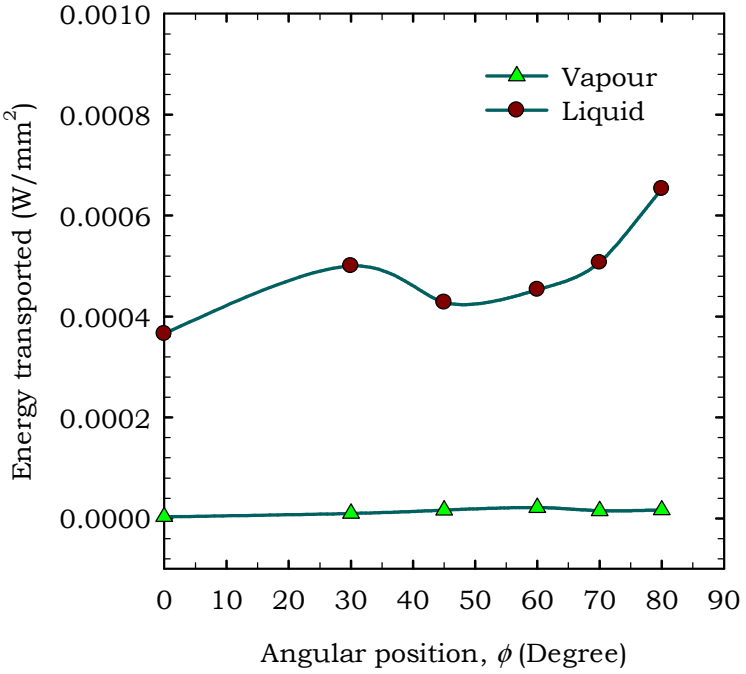

Figure 4.26 Contribution of the liquid and the vapour phases in conduction energy transport (Case-III).

For this case, a comparative plot of the rate of energy conducted through the liquid phase and the vapour phase is shown in the Figure 4.26. Unlike Case (I) and (II), the rate of energy conducted through the liquid phase, maintains a primarily increasing trend from the apex of the droplet to the three phase contact line. However, like all other cases, the contribution of the liquid phase is still higher near the three phase contact line. The vapour curve of the plot, shows that the

contribution of the vapour phase in the conduction energy transport is positive throughout the droplet, but the value is still negligible compared to the contribution of the liquid phase.

4.3.3 The evaporation rate associated with the conduction energy transport -Case (III)

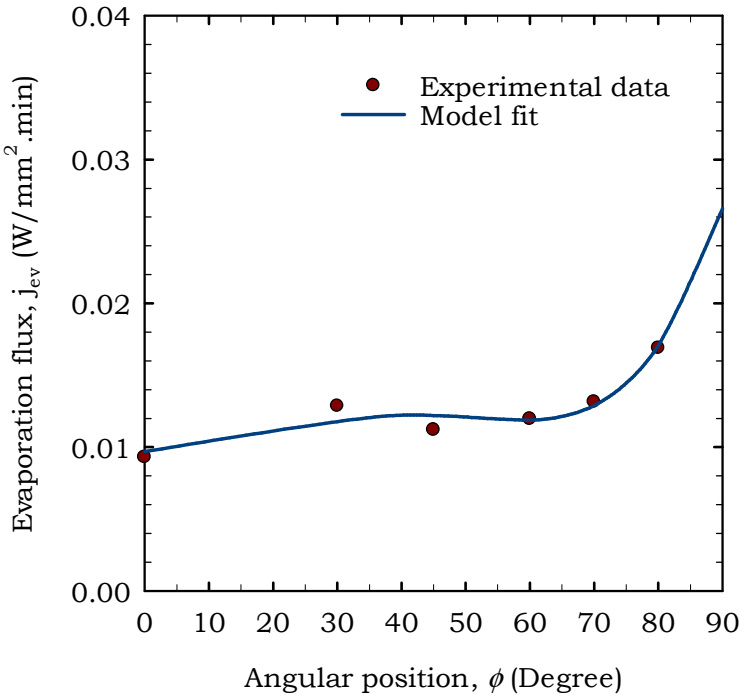

Figure 4.27 The local evaporation flux distribution from the apex to the three phase contact line (Case-III).

The local evaporation flux at different positions is shown in the Figure 4.27, the data points were fitted with a third order polynomial of "cos∅", which is $j_{ev}(\emptyset)$= 0.0266-0.0741 $\cos(\emptyset)$+0.1214$cos^2(\emptyset)$-0.0642$cos^3(\emptyset)$ for Case (III). Unlike case (I) and case

(II), the polynomial fitting of the local evaporation flux follows a primarily increasing trend from the apex to the three phase contact line of the droplet. From the apex to $\emptyset = 60°$ this slope is low, but in the region $60° < \emptyset \leq 90°$ there is a drastic increase in the slope of the fitting. It shows that the local evaporation flux in this region is higher than rest of the region of the droplet. However, like case (I) and (II), the local evaporation flux near the three phase contact line is the maximum.

In this case, the total evaporation rate associated with the conduction energy transport $'J_{ev}'$ was calculated as 0.546 μL/min and the actual evaporation rate obtained from the syringe pump was 0.85 μL/min. It shows that the evaporation rate associated with the conduction energy transport is around 64% of the actual evaporation rate. A comparison can be made between the Case (I) and (III), with same ambient temperature when the temperature of the substrate decreases from 60℃ to 32℃, the contribution of the conduction energy transport to the interfacial energy transport decreased from 91% to 64 %. Therefore, it can be concluded that for the same ambient condition a decrease in the substrate temperature causes a decrease in the conduction energy transport, and similarly other modes of interfacial energy transport become dominant over conduction energy transport.

4.3.4 Internal convective flows of the droplet -Case (III)

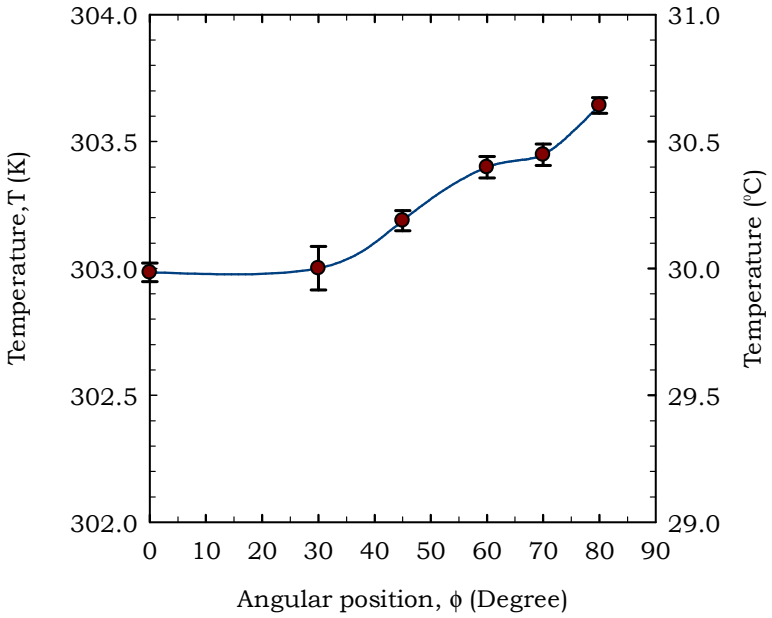

Figure 4.28 Surface temperature distribution from the apex to the three phase contact line (Case-III).

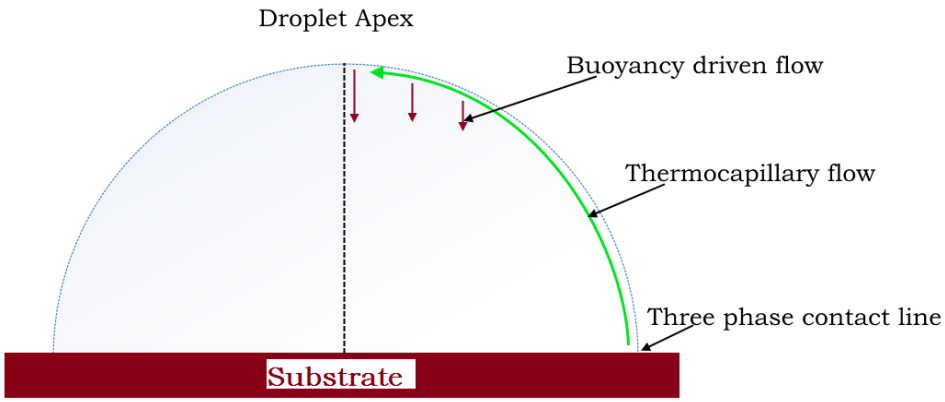

Figure 4.29 Estimated directions of the internal convection (Case-III).

Like case (I) and (II), the interfacial liquid phase temperature was recorded for different position of the droplet surface and it is shown in the Figure 4.28. The plot shows that there is a gradual increase in the surface temperature from the droplet apex to the three phase contact line. Therefore, in this case, unlike the Case (I) and (II), there will be only one cell of thermocapillary flow, and there will be a buoyancy driven convection as the apex of the droplet is colder than at the three phase contact line. In this case, a single convection cell will occur which is a combination of buoyancy driven flow and the thermocapillary flow, shown in Figure 4.29.

4.4 Case (IV) - Low substrate temperature and high ambient temperature.

In the other three cases, Case (I), case (II) and case (III), the conduction energy transport through the liquid phase was dominant, because the substrate temperature was always kept higher than the ambient temperature. In this case, the temperature of the substrate was maintained at 29.5℃ and the ambient temperature was maintained at 40℃, therefore the substrate temperature is sufficiently lower than the ambient temperature. The main purpose of choosing these temperatures for the substrate and the ambient is to observe the energy transport mechanism in the spherical droplet when the contribution of the liquid phase is expected to be low.

Like the other cases, the experiment was conducted under atmospheric pressure. All the physical phenomena analyzed and discussed in Case (I) are also analyzed in this case.

4.4.1 Temperature profile in the liquid and the vapour phases -Case (IV)

In this case, like all other cases, the temperature profiles of both the liquid and the vapour phases are plotted at both sides of the interface in Figures 4.30 to 4.35 for $\emptyset = 0°$, 30°, 45°, 60°, 70° and 80° respectively. Unlike all other cases, in this case, the temperature profiles of the liquid phase show unique patterns, where the liquid phase transports energy to the interface only at $\emptyset = 70°$ and 80°, and the rest of the region $0° \leq \emptyset < 70°$ shows a positive slope of the temperature profile of the liquid phase. This indicates that the liquid phase takes energy from the interface in this region. However, the temperature profiles of the vapour phase show a positive slope at each position. Therefor the vapour phase contributes energy to the interface throughout the surface of the droplet. The slopes of the vapour phase temperature profiles decrease when it approaches toward the three phase contact line. The reason is, unlike the case (I), this time the substrate temperature is lower than the ambient temperature, so the colder substrate cools down the vapour phase close to the bottom of the droplet.

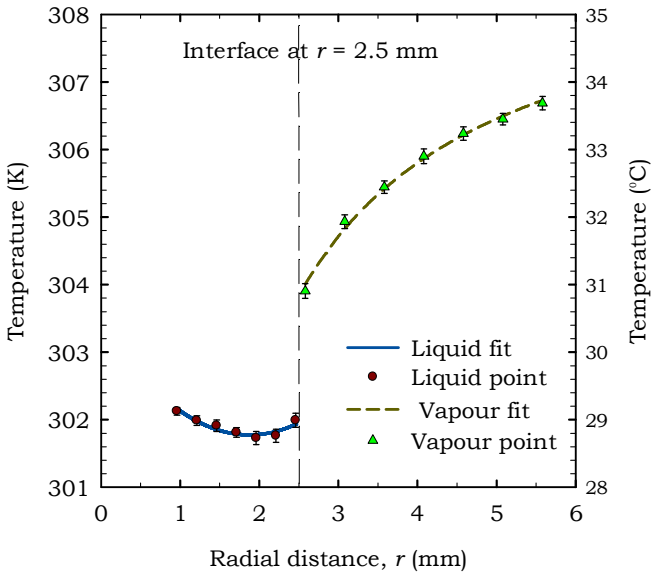

Figure 4.30 The liquid and vapour temperature profile at $\emptyset = 0°$ (Case-IV).

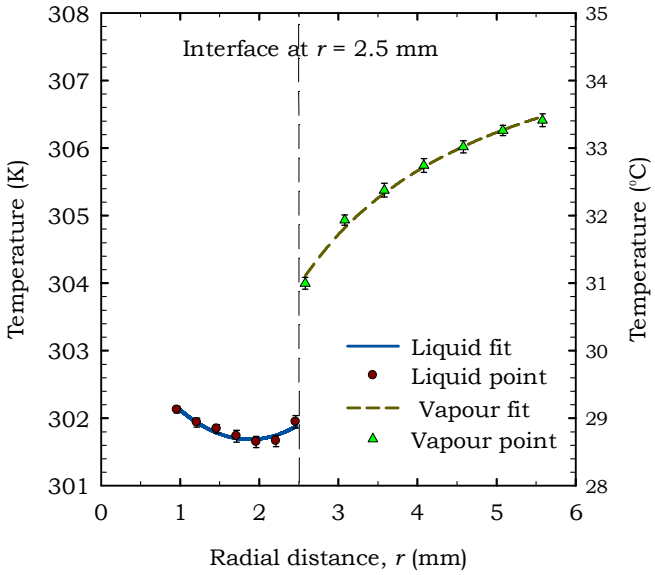

Figure 4.31 The liquid and vapour temperature profile at $\emptyset = 30°$ (Case-IV).

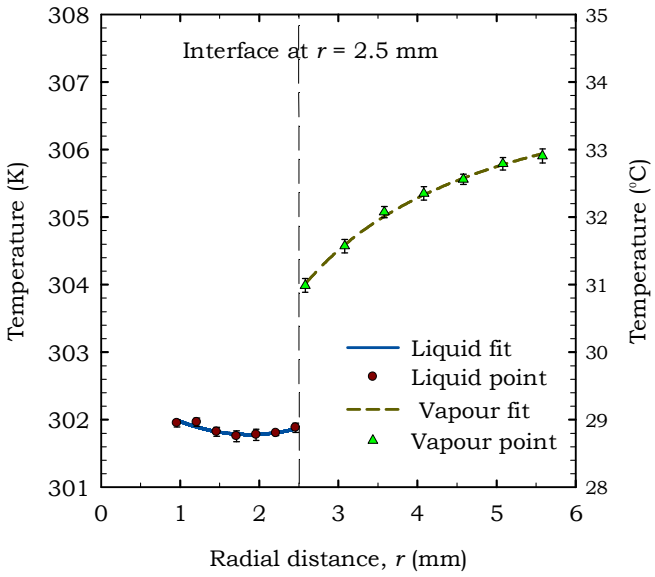

Figure 4.32 The liquid and vapour temperature profile at $\emptyset = 45°$ (Case-IV).

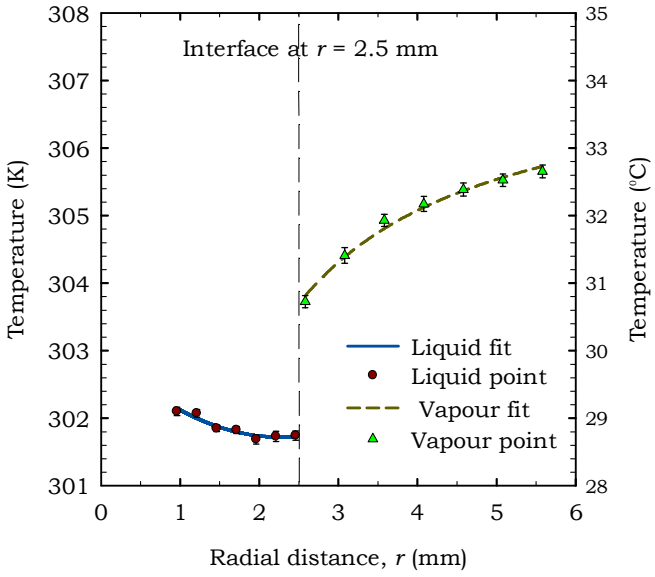

Figure 4.33 The liquid and vapour temperature profile at $\emptyset = 60°$ (Case-IV).

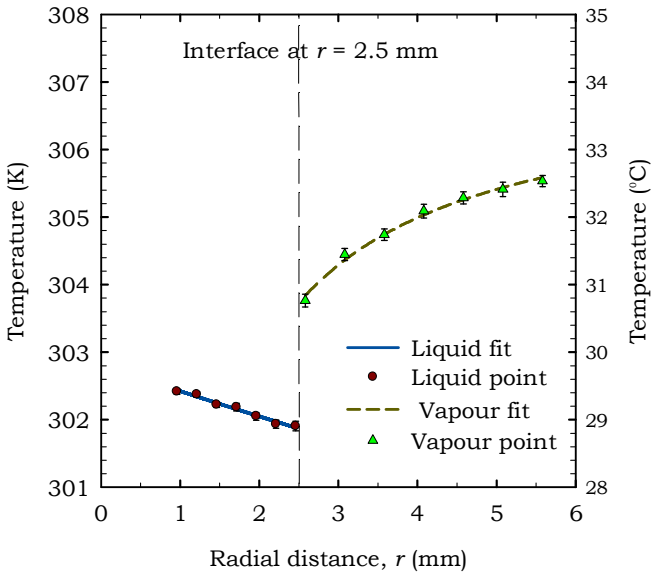

Figure 4.34 The liquid and vapour temperature profile at $\emptyset = 70°$ (Case-IV).

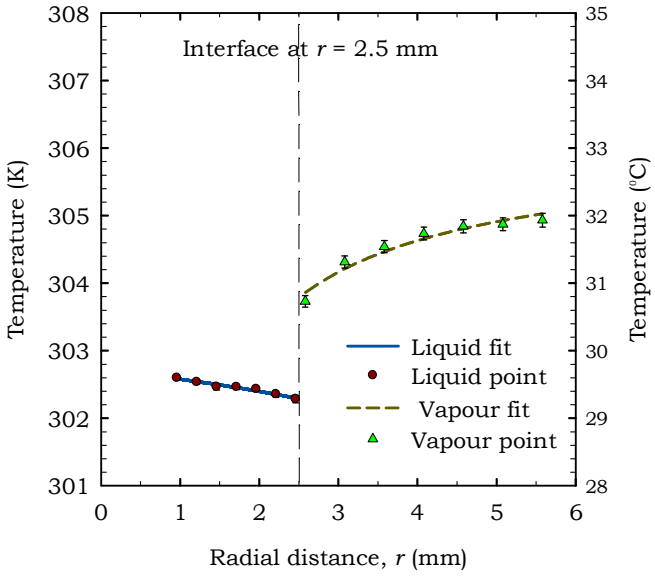

Figure 4.35 The liquid and vapour temperature profile at $\emptyset = 80°$ (Case-IV).

The temperature discontinuities at different position are shown in Figures 4.30 to 4.35. Unlike all other cases, in this case, a temperature discontinuity of around of around 2℃ was found in every position along the surface of the droplet. In each position, the interfacial vapour temperature is higher than the interfacial liquid temperature. This large temperature discontinuity at the interface can affect the conventional conduction energy transport mechanism.

4.4.2 Contribution of the liquid and the vapour phases in the conduction energy transport -Case (IV).

For this case, Figure 4.36 shows the comparative contribution of the vapour and the liquid phases at different position of the droplet. Since the ambient temperature is high and the temperature of the substrate is low, before the experiment it was expected that the contribution of the vapour phase will be significant in this case. However, the plot shows that still in this case, the contribution of the vapour phase in the conduction energy transport is equally negligible, and it decreases from the droplet apex to the three phase contact line. The liquid contribution curve in Figure 4.36 shows unique characteristics compared to all the other cases. It shows that, the liquid phase takes energy from the interface in the region $0° \leq \emptyset \leq 60°$ and it contributes in the energy conduction to the interface only in the region $70° \leq \emptyset \leq 90°$, but in this region, unlike all other cases, there is a decreasing trend of this

contribution. So it can be concluded that the contributions of the liquid and the vapour phases in the conduction energy transport to the interface, are equally negligible in a condition where the temperature is low and the ambient temperature is high.

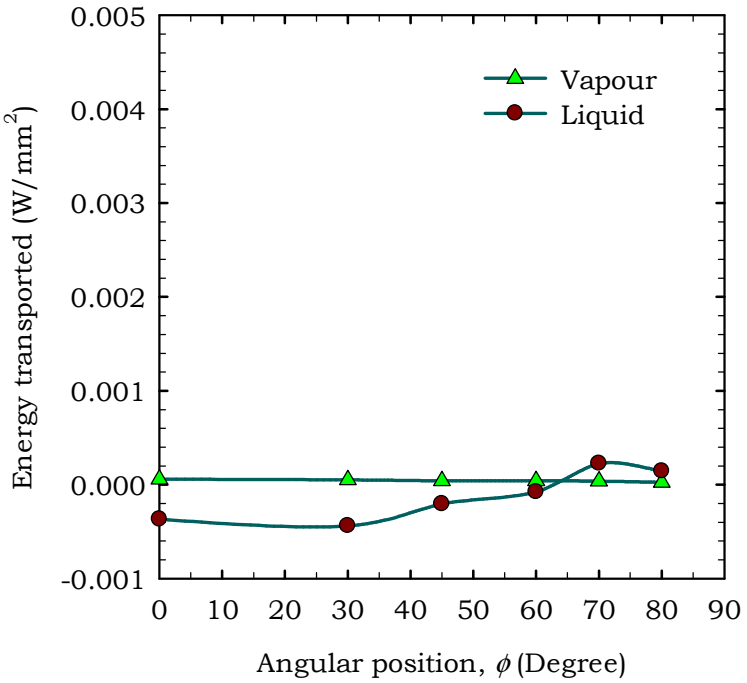

Figure 4.36 Contribution of the liquid and the vapour phases in conduction energy transport (Case-IV).

4.4.3 The evaporation rate associated with the conduction energy transport -Case (IV).

Figure 4.37 shows the local evaporation flux at different positions, the data points were fitted with a third order polynomial of "cos∅", which is $j_{ev}(\emptyset)$= -0.0046+0.0084 $\cos(\emptyset)$-0.2059$cos^2(\emptyset)$+0.1172$cos^3(\emptyset)$ in Case (IV). In the previous section it is discussed that, in this case, the contribution of both the liquid

and the vapour phases is almost negligible as shown in Figure 4.36. Therefore the local evaporation fluxes, associated with the conduction energy transport through the liquid and the vapour phase, are also almost negligible, shown in Figure 4.37. However, in the region$0° \leq \emptyset \leq 60°$, the local evaporation fluxes are slightly negative, as seen in Figure 4.37, which indicate that if the conduction energy transport was the only mode of energy transport to this region then there would be some condensation. In the region$70° \leq \emptyset \leq 90°$, the local evaporation fluxes are positive, but unlike all other cases, it is decreasing towards the three phase contact line.

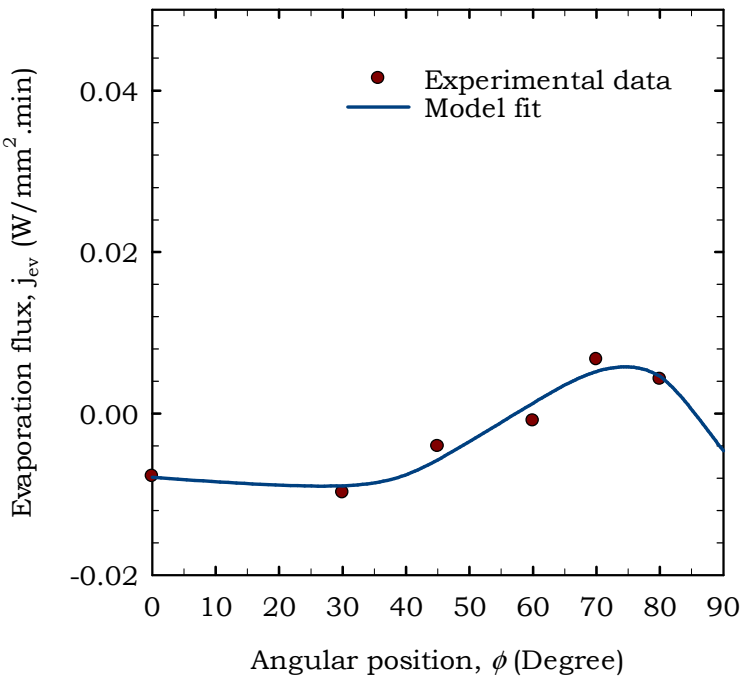

Figure 4.37 The local evaporation flux distribution from the apex to the three phase contact line (Case-IV).

In this case, the total evaporation rate associated with the conduction energy transport $'J_{ev}'$ was calculated as -0.039 μL/min, whereas the actual evaporation rate obtained from the syringe pump was 0.55 μL/min. The evaporation rate associated with the conduction energy transport is showing that there will be condensation in this case, but the actual evaporation rate is showing evaporation like Case (III). Therefore the conduction energy transport to the interface through the liquid and the vapour phases cannot explain the evaporation situation, where the temperature of the substrate is low and the ambient temperature is high. In this case, other modes of the energy transport likely play a significant role in the interfacial energy transport.

4.4.4 Internal convective flows of the droplet -Case (IV).

The plot for the temperature distribution of the interfacial liquid phase along the droplet surface is shown in Figure 4.38. The shape of this temperature distribution plot is similar to Case (I) but the magnitude is lower. Like case (I) and case (II), the apex of the droplet (∅=0°) will also be colder than droplet bottom (∅=90°) which is apparent from the plot. A similar buoyancy driven flow and two thermocapillary flows will form inside the droplet, shown in Figure 4.10. These internal convective flows are responsible for the interfacial energy transport. In addition, since the

ambient temperature is high and the temperature of the internal surfaces of the enclosure is also high, there will also be radiation energy transport to the interface.

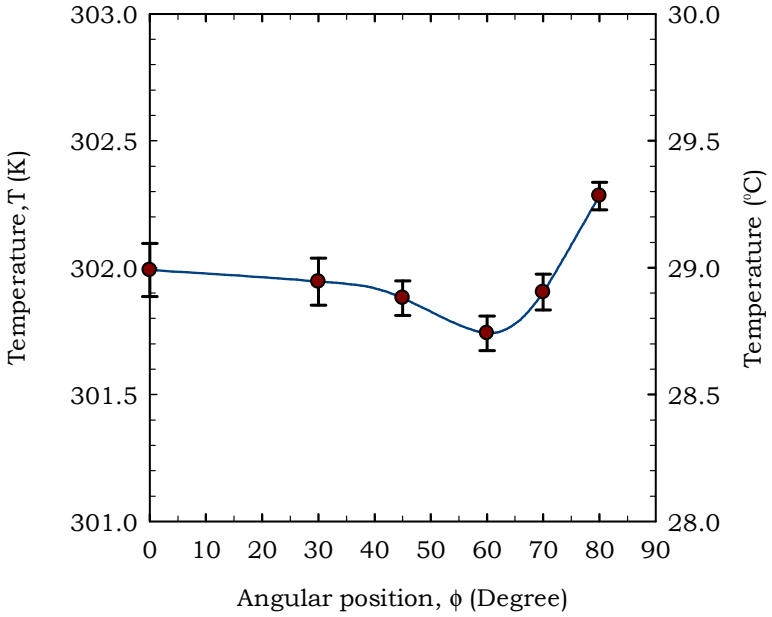

Figure 4.38 Surface temperature distribution from the apex to the three phase contact line (Case-IV).

4.5 Comparative analysis on the interfacial energy transport in all four cases

Figure 4.39 shows the evaporation flux distribution along the droplet interface for all four cases and Table 4.2 shows the contribution of conduction energy transport in those cases. From the plot of evaporation flux distribution it is apparent that the

evaporation rates associated with the conduction decrease from Case (I) to (IV), because local evaporation fluxes decrease from Case (I) to (IV).

Table 4.2 Contribution of the conduction energy transport in cases.

		Case-I	Case-II	Case-III	Case-IV
J_{actual} (μL/min)	<syringe pump>	4.60±0.02	4.35±0.02	0.85±0.004	0.55±0.003
J_{ev} (μL/min)	<conduction>	4.19	2.93	0.55	-0.04
Contribution of the conduction energy transport		91%	67%	64%	-

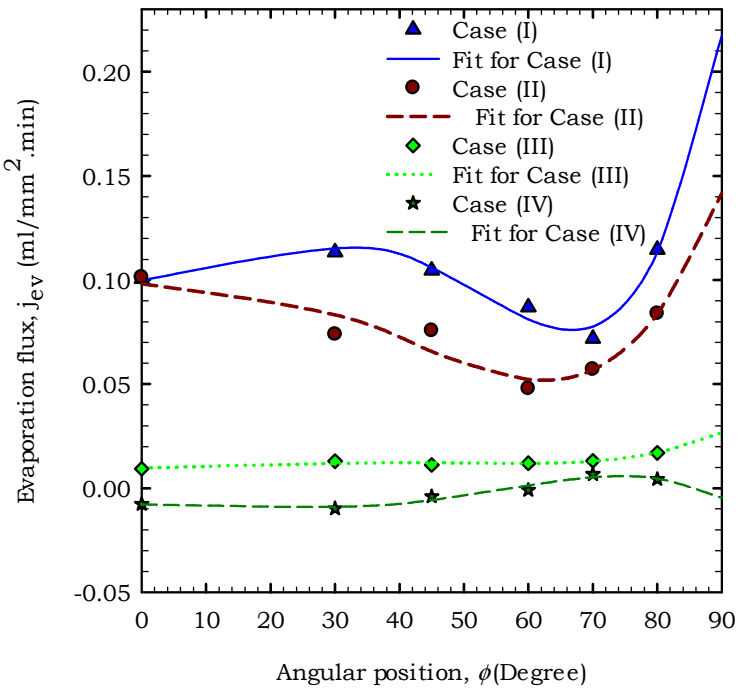

Figure 4.39 Comparison of the local evaporation flux distribution from the apex to the three phase contact line for all four cases.

Analysis on Case (I) shows that, conduction energy transport is dominant when the substrate temperature is high and surrounding is low. In this case the conduction energy transport contributes 91% of total required energy. However, Case (II) shows that for the same substrate temperature (60℃) conduction energy transport contributes less with increase in surrounding temperature from 30℃ to 40℃. In this case conduction contributes about 67% of total energy required at the interface. It indicates that an increase in surrounding temperature may suppress the conduction energy transport and enhance other modes of energy transport to the interface, such as energy transport by thermocapillary flow and buoyancy driven flow. In Case (III) both the substrate temperature and enclosure temperature were maintained close to room temperature, but the substrate temperature was slightly higher than the ambient temperature. In this case, conduction energy transport contributes 64 % to the total energy required at the interface, which indicates that a decrease in substrate temperature makes conduction energy transport contributes less of the total energy requirement at the interface. In case (IV), conduction energy transport is almost negligible, and a negative value of evaporation flux indicates probable condensation at the interface, but actually there is a substantial evaporation rate at the interface. Therefore in practical situations when the substrate temperature is low and the surrounding temperature is high, the internal convections may become dominant. In

addition, depending on the relative direction of droplet internal flow and thermal conduction, in some regions the internal convection may suppress thermal conduction and in some region, it may enhance thermal conduction.

Temperature discontinuity along the interface plays a significant role in the interfacial energy transport [26]. The relative temperature of the liquid and vapour phases and estimated temperature discontinuities obtained from the plots are summarized in Table 4.3. The temperature profiles of Case (I) show that the interfacial liquid phase temperature is consistently greater than the interfacial vapour temperature and the magnitude of the temperature discontinuity is high, and this is the most conduction dominant case. In contrast, temperature profiles of Case (IV) show that the interfacial liquid phase temperature is consistently lower than the interfacial vapour temperature and the magnitude of the temperature discontinuity is high, and in this case contribution of conduction is negative, so other modes of energy transport, such as internal convections, are dominating. Therefore situations with high temperature discontinuity that is consistent along the interface corresponds to a dominant energy transport mode, as shown in Table 4.2 and 4.3.

Table 4.3 The temperature discontinuities found from the temperature profiles of the liquid and vapour phases.

Case	Relative temperature at interface		Temperature discontinuity
	Near Apex	Near three phase contact line	
I	$T_i^V < T_i^L$	$T_i^V < T_i^L$	1~ 2.5℃
II	$T_i^V < T_i^L$	$T_i^V > T_i^L$	<1 ℃
III	$T_i^V > T_i^L$	$T_i^V < T_i^L$	<0.5℃
IV	$T_i^V > T_i^L$	$T_i^V > T_i^L$	2~ 2.5℃

In Case (II) and (III), the conduction energy transport contributes more that 60%, but there is a substantial contribution from other energy transport modes, such as internal convections. In both cases, the temperature discontinuity is low and the direction of the temperature discontinuity changes along the droplet surface. Therefore, it is apparent that, situations with a small temperature discontinuity along the interface corresponds to a combined energy transport by conduction and other modes of energy transport as shown in the Table 4.2 and 4.3 .

Chapter 5

5 CONCLUSION

The detailed observations are explained in the previous chapter. However, in this chapter final findings from the experiments are summarized along with the recommendations for future work. Summary of the objectives of this thesis needs to be mentioned in this chapter again to place the conclusion in context. The objectives of this thesis are the followings:

i. Determine the energy transport and internal flow in an evaporating sessile droplet for practical conditions
    a. Measure temperature profiles of the liquid and vapour phases to understand the energy transport mechanisms.
    b. Calculate the local evaporation flux along the droplet surface.

ii. Determine if there is any temperature discontinuity in practical applications.

5.1 Conclusions

Under static ambient condition, the evaporation rate is dominated by the substrate temperature, at high substrate temperature the evaporation rate is high, and vice versa. Conduction energy transport is dominant in the case of high substrate temperature and low ambient temperature (Case-I). For the same low ambient temperature, the contribution of the conduction energy transport decreases with decreasing substrate temperature (Case-III). In case of high substrate temperature and high ambient temperature, the contribution of the conduction energy transport is high but there is a significant contribution of the internal convections (case-II). For the same hot ambient, the contribution of the conduction energy transport decreases with the decreasing substrate temperature (case IV). In addition, a sessile droplet can have single convection cell (Case III) or multiple convection cell (Case I, II and IV) inside the droplet depending on the temperature conditions.

The temperature discontinuity varies with the substrate and ambient conditions. If interfacial liquid phase temperature is consistently higher than the interfacial vapour phase temperature and the magnitude of the discontinuity is high, it indicates the dominant conduction energy transport (Case I), and vice versa (case IV). A small temperature discontinuity with inconsistent direction along the surface,

shows the combined energy transport of conduction and internal convections (Case II and III).

This experimental investigation shows that the energy transport mechanism in a spherical sessile droplet is complex, and the dominant mode of energy transport varies with the substrate and ambient temperature conditions. Therefore, the design of an evaporative cooling system with spherical sessile droplets, must factor in conduction and other modes of energy transport depending on the practical temperature conditions.

5.2 Recommendation for future work

In this research work, all the experiments were conducted with the copper substrate and the thermal conductivity of copper is very high. Therefore, these experiments do not provide information about the evaporation of a sessile droplet on a substrate with a low thermal conductivity. Further experimental investigations are required to understand the effect of substrate thermal conductivity on the evaporation tare.

In this research work, distilled water was used as the liquid throughout the experiment, but some research work found that thermal conductivity of the liquid can affect the internal convections. Therefore, other liquids suitable for the phase

change applications, can be investigated for the optimum design of evaporative cooling systems.

Another factor, the droplet size, was constant throughout the experiments, but droplet size can significantly affect the evaporation. It can alter the evaporation flux as well the internal convections. Therefore further investigation is required to find out the effect of droplet size under different experimental condition.

In this research work, the direction of internal convections were explained with the help of the surface temperature distribution. However, the flow visualization and the speed of the flow are essential for proper understanding of the energy transport by the internal convection. Further work needs to be done on the evaporation of the spherical shape sessile droplet with proper visualization and speed measurement technique, such as the Particle Image Velocimetry (PIV) system. PIV system can help to visualize the flow direction and it can measure the speed of the internal convection, but this kind of visualization technique can affect the properties of the liquid.

The natural evaporative cooling system, such as human perspiration system, works better with forced convection. Therefore, the evaporation of the sessile droplet

under forced convection should investigated to implement droplet evaporation technology in evaporative cooling systems.

References

1. Ytrehus, T. and S. Østmo, *Kinetic theory approach to interphase processes.* International Journal of Multiphase Flow, 1996. **22**(1): p. 133-155.
2. Bond, M. and H. Struchtrup, *Mean evaporation and condensation coefficients based on energy dependent condensation probability.* Physical Review E, 2004. **70**(6): p. 061605.
3. Yu, J. and H. Wang, *A molecular dynamics investigation on evaporation of thin liquid films.* International Journal of Heat and Mass Transfer, 2012. **55**(4): p. 1218-1225.
4. Ghasemi, H. and C.A. Ward, *Energy Transport by Thermocapillary Convection during Sessile-Water-Droplet Evaporation.* Physical Review Letters, 2010. **105**(13): p. 136102.
5. Carey, V.P., *Liquid vapor-Phase-Change Phenomena*, ed. Second. 2007, New York, USA: Taylor & Francis group.
6. Hendarto, E. and Y.B. Gianchandani, *Size sorting of floating spheres based on Marangoni forces in evaporating droplets.* Journal of Micromechanics and Microengineering, 2013. **23**(7): p. 075016.
7. Ristenpart, W.D., et al., *Influence of Substrate Conductivity on Circulation Reversal in Evaporating Drops.* Physical Review Letters, 2007. **99**(23): p. 234502.
8. Niazmand, H., et al., *Effects of Marangoni Convection on Transient Droplet Evaporation.* Combustion Science and Technology, 1994. **103**(1-6): p. 219-233.
9. Ward, C.A. and G. Fang, *Expression for predicting liquid evaporation flux: Statistical rate theory approach.* Physical Review E - Statistical Physics, Plasmas, Fluids, and Related Interdisciplinary Topics, 1999. **59**(1): p. 429-440.
10. Fang, G. and C.A. Ward, *Examination of the statistical rate theory expression for liquid evaporation rates.* Physical Review E, 1999. **59**(1): p. 441-453.
11. Ward, C.A. and D. Stanga, *Interfacial conditions during evaporation or condensation of water.* Physical Review E, 2001. **64**(5): p. 051509.
12. Hu, H. and R.G. Larson, *Evaporation of a Sessile Droplet on a Substrate.* The Journal of Physical Chemistry B, 2002. **106**(6): p. 1334-1344.
13. David, S., K. Sefiane, and L. Tadrist, *Experimental investigation of the effect of thermal properties of the substrate in the wetting and evaporation of sessile drops.* Colloids and Surfaces A: Physicochemical and Engineering Aspects, 2007. **298**(1–2): p. 108-114.

14. Dunn, G.J., et al., *A mathematical model for the evaporation of a thin sessile liquid droplet: Comparison between experiment and theory.* Colloids and Surfaces A: Physicochemical and Engineering Aspects, 2008. **323**(1–3): p. 50-55.
15. Dunn, G.J., et al., *The strong influence of substrate conductivity on droplet evaporation.* Journal of Fluid Mechanics, 2009. **623**: p. 329-351.
16. Sefiane, K., et al., *On the effect of the atmosphere on the evaporation of sessile droplets of water.* Physics of Fluids (1994-present), 2009. **21**(6): p. -.
17. Girard, F., M.l. Antoni, and K. Sefiane, *Infrared Thermography Investigation of an Evaporating Sessile Water Droplet on Heated Substrates.* Langmuir, 2010. **26**(7): p. 4576-4580.
18. Hu, H. and R.G. Larson, *Analysis of the Microfluid Flow in an Evaporating Sessile Droplet.* Langmuir, 2005. **21**(9): p. 3963-3971.
19. Xu, X. and J. Luo, *Marangoni flow in an evaporating water droplet.* Applied Physics Letters, 2007. **91**(12): p. -.
20. Girard, F., et al., *Influence of heating temperature and relative humidity in the evaporation of pinned droplets.* Colloids and Surfaces A: Physicochemical and Engineering Aspects, 2008. **323**(1–3): p. 36-49.
21. Starov, V. and K. Sefiane, *On evaporation rate and interfacial temperature of volatile sessile drops.* Colloids and Surfaces A: Physicochemical and Engineering Aspects, 2009. **333**(1–3): p. 170-174.
22. Christy, J.R.E., K. Sefiane, and E. Munro, *A Study of the Velocity Field during Evaporation of Sessile Water and Water/Ethanol Drops.* Journal of Bionic Engineering, 2010. **7**(4): p. 321-328.
23. Sefiane, K., *On the Formation of Regular Patterns from Drying Droplets and Their Potential Use for Bio-Medical Applications.* Journal of Bionic Engineering, 2010. **7, Supplement**(0): p. S82-S93.
24. Xu, X., J. Luo, and D. Guo, *Criterion for Reversal of Thermal Marangoni Flow in Drying Drops.* Langmuir, 2010. **26**(3): p. 1918-1922.
25. MacDonald, B.D. and C.A. Ward, *Onset of Marangoni convection for evaporating liquids with spherical interfaces and finite boundaries.* Physical Review E, 2011. **84**(4): p. 046319.
26. MacDonald, B.D. and C.A. Ward, *Onset of Marangoni convection for evaporating sessile droplets.* Journal of Colloid and Interface Science, 2012. **383**(1): p. 198-207.
27. Xu, X., et al., *Linear growth of colloidal rings at the edge of drying droplets.* Colloids and Surfaces A: Physicochemical and Engineering Aspects, 2014. **447**(0): p. 28-31.
28. Xu, X. and L. Ma, *Analysis of the effects of evaporative cooling on the evaporation of liquid droplets using a combined field approach.* Scientific Reports, 2015. **5**.

29. Sefiane, K. and C.A. Ward, *Recent advances on thermocapillary flows and interfacial conditions during the evaporation of liquids.* Advances in Colloid and Interface Science, 2007. **134–135**(0): p. 201-223.
30. Ward, C.A. and F. Duan, *Turbulent transition of thermocapillary flow induced by water evaporation.* Physical Review E, 2004. **69**(5): p. 056308.
31. Duan, F. and C.A. Ward, *Surface excess properties from energy transport measurements during water evaporation.* Physical Review E - Statistical, Nonlinear, and Soft Matter Physics, 2005. **72**(5).
32. Duan, F., et al., *Thermocapillary transport of energy during water evaporation.* Physical Review E - Statistical, Nonlinear, and Soft Matter Physics, 2005. **72**(5).
33. Duan, F. and C.A. Ward, *Investigation of Local Evaporation Flux and Vapor-Phase Pressure at an Evaporative Droplet Interface.* Langmuir, 2009. **25**(13): p. 7424-7431.
34. Sobac, B. and D. Brutin, *Thermocapillary instabilities in an evaporating drop deposited onto a heated substrate.* Physics of Fluids, 2012. **24**(3).
35. Sobac, B. and D. Brutin, *Thermal effects of the substrate on water droplet evaporation.* Physical Review E, 2012. **86**(2): p. 021602.